RESEARCH ARTICLE

THE PROTEIN SOCIETY WILEY

Dynamic proximity interaction profiling suggests that YPEL2 is involved in cellular stress surveillance

Gizem Turan[1] | Çağla Ece Olgun[1] | Hazal Ayten[1] | Pelin Toker[1] | Annageldi Ashyralyyev[1] | Büşra Savaş[2,3] | Ezgi Karaca[2,3] | Mesut Muyan[1,4]

[1]Department of Biological Sciences, Middle East Technical University, Ankara, Türkiye

[2]İzmir Biomedicine and Genome Center, İzmir, Türkiye

[3]Izmir International Biomedicine and Genome Institute, Dokuz Eylül University, Izmir, Türkiye

[4]CanSyl Laboratories, Middle East Technical University, Ankara, Türkiye

Correspondence

Mesut Muyan, Department of Biological Sciences, Middle East Technical University, Ankara, Türkiye.
Email: mmuyan@metu.edu.tr

Review Editor: Aitziber L. Cortajarena

Abstract

YPEL2 is a member of the evolutionarily conserved YPEL family involved in cellular proliferation, mobility, differentiation, senescence, and death. However, the mechanism by which YPEL2, or YPEL proteins, mediates its effects is largely unknown. Proteins perform their functions in a network of proteins whose identities, amounts, and compositions change spatiotemporally in a lineage-specific manner in response to internal and external stimuli. Here, we explored interaction partners of YPEL2 by using dynamic TurboID-coupled mass spectrometry analyses to infer a function for the protein. Our results using inducible transgene expressions in COS7 cells indicate that proximity interaction partners of YPEL2 are mainly involved in RNA and mRNA metabolic processes, ribonucleoprotein complex biogenesis, regulation of gene silencing by miRNA, and cellular responses to stress. We showed that YPEL2 interacts with the RNA-binding protein ELAVL1 and the selective autophagy receptor SQSTM1. We also found that YPEL2 localizes stress granules in response to sodium arsenite, an oxidative stress inducer, which suggests that YPEL2 participates in stress granule-related processes. Establishing a point of departure in the delineation of structural/functional features of YPEL2, our results suggest that YPEL2 may be involved in stress surveillance mechanisms.

KEYWORDS

ELAVL1, proximity interactions, SQSTM1, TurboID, YPEL2

1 | INTRODUCTION

In an effort directed at deciphering the underlying mechanism of 17β-estradiol (E2)-estrogen receptors α (ERα)

actions at genomic levels, we previously identified *Yippee Like 2* (*YPEL2*) as an E2-ERα responsive gene (Nott et al., 2009). The yippee protein of *Drosophila melanogaster* was first described in a yeast interaction trap screen as a protein physically interacting with the hemolin protein of *Hyalophora cecropia* (Roxström-Lindquist & Faye, 2001). Subsequent studies with the sequencing of a

Gizem Turan and Çağla Ece Olgun contributed equally to this study and should be considered as the first authors.

cDNA library generated from total RNA from mouse embryonic branchial arch tissue, which is an integral part of the development of the craniofacial complex, led to the identification of a cDNA of 2396 bp in length, with a single open reading frame (ORF) of 357 bp encoding 119 residue Yippee-like 1 (Ypel1) protein that shows very high amino-acid sequence homology to the Yippee protein (Farlie et al., 2001). Screening of the human expressed sequence tag (EST) with a mouse Ypel1 ORF probe identified the human YPEL1 gene that maps to human chromosome 22q11.2, a region associated with several congenital anomalies involving craniofacial malformation including DiGeorge syndrome and Velocardiofacial syndrome (Sullivan, 2001). Sequence comparison at nucleotide levels indicated a high degree of conservation (91.2%) between the human YPEL1 and mouse Ypel1 ORFs and among many vertebrate and non-vertebrate species (Farlie et al., 2001). Similarly, a differential gene expression analysis of 32Dcl3 myeloblastic cells in the presence or absence of interleukin 3 identified a gene that encodes the small unstable apoptotic protein (SUAP), which is now named YPEL3, as a homolog of Yippee and Ypel1 (Baker, 2003). Later studies using the YPEL1 cDNA as a query sequence for the entire human genome revealed four paralogs with remarkably high nucleotide sequence homologies on four different chromosomes: YPEL2 (17q23.2), YPEL3 (16p11.2), YPEL4 (11q12.1), and YPEL5 (2q23.1) giving rise to the YPEL gene family (Hosono et al., 2004). Although the number of YPEL genes varies with species, they are expressed essentially in all eukaryotes (Hosono et al., 2004, 2010).

The YPEL family genes encode small proteins with molecular masses (MMs) ranging from 13.5 to 17.5 kDa, showing remarkably high amino-acid sequence identities (43.8%–96.6%). Amino-acid sequence alignments based on the highly conserved cysteine residues of all identified YPEL proteins in different species revealed two cysteine pairs that are 52 amino acids apart ($C\text{-}X_2\text{-}C\text{-}X_{52}\text{-}C\text{-}X_2\text{-}C$) predicted to form a zinc-finger like metal binding pocket, or the Yippee domain (Baker, 2003; Nott et al., 2009). This high evolutionary conservation among YPEL proteins implies that YPELs are critically involved in various cellular processes. Indeed, experimental studies suggest that the YPEL proteins, including YPEL2, participate in cellular proliferation, mitochondrial function, morphology, mobility, differentiation, senescence, and death (Aerts et al., 2006a; Blanco-Sanchez et al., 2020; Farlie et al., 2001; Garcıá et al., 2019; Hosono et al., 2004, 2010; Jun et al., 2007; K. D. Kelley et al., 2010; J. H. Kim et al., 2020; Kong et al., 2018; J. Y. Lee et al., 2017; W. Li et al., 2022; Liang et al., 2010; Mattebo et al., 2021; Oki et al., 2016; Sullivan, 2001; Tan et al., 2015; Tuttle et al., 2012; J. Zhang et al., 2016). Moreover, deregulated expression of YPEL genes could be associated with, or contribute to, the initiation/development of various disorders, malignancies, and resistance to therapies (Blanco-Sanchez et al., 2020; Hosono et al., 2010; S. Li et al., 2019; W. Li et al., 2022; Mattebo et al., 2021; Tuttle et al., 2011; Vysotskiy et al., 2021; L. Wang et al., 2022; Wu, 2018). Similarly, high levels of YPEL2 expression are suggested to contribute to Dominant Retinitis Pigmentosa (Y. Li et al., 2021), atherosclerosis (Y. Li et al., 2021), autophagy processes in breast cancer (de Bruijn et al., 2020), and improved overall survival of clear cell renal cell carcinoma (ccRCC) patients (J. Y. Lee et al., 2017). However, the mechanisms by which YPEL proteins mediate their effects are yet unclear. Proteins perform their functions in a network of proteins whose identities, amounts, and compositions change spatiotemporally in a lineage-specific manner in response to various internal and external stimuli (Greene, 2012; Mascia et al., 2022). To better understand the functional features of YPEL2 in mediating cellular processes in physiology and pathophysiology, we initially explored the identification of protein interaction networks of YPEL2 dynamically. Using inducible transgene expression in COS7 cells followed by time-resolved TurboID-coupled mass spectrometry (MS) analyses, we found that YPEL2 proximity interacts with proteins mainly involved in RNA and mRNA metabolic processes, ribonucleoprotein complex biogenesis, regulation of gene silencing by miRNA, and cellular responses to stress. We also found that YPEL2, as endogenous YPEL proteins in COS7 cells, localizes in stress granules in response to sodium arsenite (SA), an oxidative stress inducer. These findings collectively suggest a crucial role for YPEL2 as a key component in cellular responses to oxidative stress, emphasizing its potential significance in stress granule-related processes.

2 | RESULTS

The human YPEL gene family contains five paralogs on five different chromosomes: YPEL1 (22q11.2), YPEL2 (17q23.2), YPEL3 (16p11.2), YPEL4 (11q12.1), and YPEL5 (2q23.1) with transcripts that display remarkably high nucleotide sequence homology (Baker, 2003) (Figures 1 and S1). In agreement with previous studies conducted with Northern blot or PCR analyses of human tissue cDNA libraries (Baker, 2003; Sullivan, 2001), our tissue-specific gene expression analyses with the GTEx portal (https://gtexportal.org/home/) (Figure S2) suggest that while *YPEL1* is expressed primarily in the brain and testis; the expression of *YPEL4* is restricted mainly to the brain. On the other hand, *YPEL2*, *3*, and *5* appear to be expressed in all tissues examined. The YPEL family genes
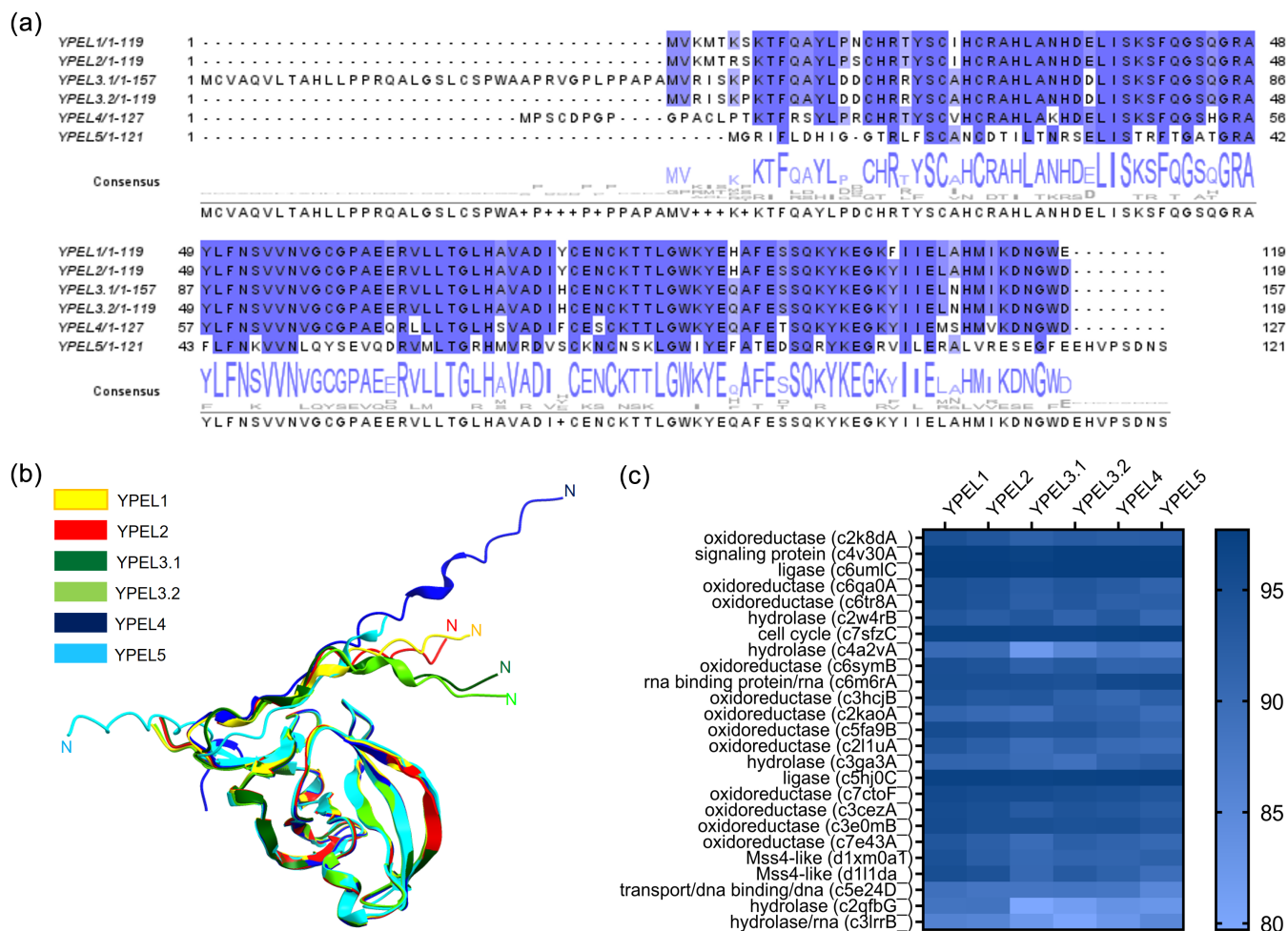
(a)

(b)

(c)

FIGURE 1 In silico analyses of YPEL proteins. (a) The alignment of amino acid sequences of YPEL proteins was generated with the Jalview program using the ClustalOmega plug-in. (b) Prediction and superimposition of tertiary structures of YPEL proteins were carried out with the AlphaFold server using the ChimeraX molecular visualization program. (c) The Phyre2 web tool was used for the homology modeling of YPEL proteins.

encode proteins with very high amino acid sequence identities such that the homology among the YPEL1-YPEL4 proteins is 83.2%–96.6%, whereas YPEL5 shows the lowest homology (43.8%) (Baker, 2003) as our analyses also indicate (Figure 1a). It should be noted that there exist two isoforms of YPEL3 resulting from alternative splicing in the first exon of YPEL3 (https://www.ncbi.nlm.nih.gov/gene?Db=gene&Cmd=DetailsSearch&Term=83719). The YPEL3 isoform2 has an additional 38 amino acids at the amino terminus, generating a 157 aa long protein with an estimated MM of 17.5. In contrast, the YPEL3 isoform1 comprises 119 amino acids with an estimated MM of 13.6 kDa. YPEL3 isoform1, YPEL1, and YPEL2 are 119 aa in length proteins with estimated MMs of 13.5 kDa. The YPEL4 protein is 127 aa in length with an estimated MM of 14.3 kDa, whereas YPEL5 comprises 121 amino acids with an estimated MM of 13.8 kDa. The extraordinarily high degree of amino-

acid sequence identity among YPEL proteins identifies a consensus sequence of $C-X_2-C-X_{19}-G-X_3-L-X_5-N-X_{13}-G-X_8-C-X_2-C-X_4-GWXY-X_{10}-K-X_6-E$ for all YPEL proteins (Baker, 2003; Nott et al., 2009). Based on the primary structures of YPEL proteins, our analyses to predict tertiary structures using the AlphaFold (Jumper et al., 2021; Spirin & Mirny, 2003) server (https://alphafold.ebi.ac.uk/) with the ChimeraX molecular visualization (Pettersen et al., 2021; Varadi et al., 2022) program (https://www.cgl.ucsf.edu/chimerax/) suggested that YPEL proteins, except the short sequences at the amino-termini, fold into a superimposable globular structure, or Yippee domain, (Figure 1b). Moreover, structural homologs of YPEL proteins using the Phyre2 (Goddard et al., 2018) server (http://www.sbg.bio.ic.ac.uk/~phyre2/html/page.cgi?id=index) to infer a potential function(s) for YPEL proteins indicated matches for YPEL proteins with probabilities of more than 80% confidence to the

Yippee-like domains of oxidoreductase, RNA binding/hydrolase, ligase/signaling, and MSS4/RABIF-like protein families (Figure 1c).

The evolutionary conservation in nucleotide sequences of ORFs, encoded amino acid sequences, and predicted functions of YPELs could point to similar activities for YPEL proteins in cellular processes. However, this also poses experimental challenges in deciphering the role of a YPEL protein when co-expressed/synthesized with other YPELs. For example, our analyses, using the Cancer Dependency Map portal (DepMap, DM, https://depmap.org/portal/), of the average expression of the YPEL gene family members in breast cancer cell lines (DM-BCCL) or only in MCF7 cells (DM-MCF7) together with our results from MCF7 cells with qPCR (MCF7) suggest that YPEL2, 3, and 5 genes are expressed in these cell lines (Figure 2a). Moreover, treatment of MCF7 cells, grown for 72 h in CD-FBS to reduce the endogenous estrogen hormone concentrations, with E2 (10^{-9} M) for 24 h led to suppression of $YPEL2$, $YPEL5$, and as shown previously for $YPEL3$ (K. D. Kelley et al., 2010), expressions compared to control cells treated with ethanol (EtOH) (Figure 2b). E2 treatment, on the other hand, augmented the expression of $TFF1$, an E2-responsive gene that we used as a control (L. A. Kelley et al., 2015). The suppression of $YPEL2$, 3, and 5 expressions is ER-dependent because 10^{-7} M Imperial Chemical Industries 182,780 (ICI), a complete ER antagonist (Yaşar et al., 2016), effectively blocked the E2-mediated repression. Thus, E2-ER signaling mediates the expression of $YPEL2$, $YPEL3$, and $YPEL5$ in MCF7 cells. These findings are similar to observations in which the suppression of $MDM4$ or $MDM2$ transcript levels involved in mediating p53 activities with a siRNA approach in MCF7 cells alters the expression of $YPEL2$, $YPEL3$, and $YPEL5$ (Wakeling & Bowler, 1987). We also observed that in COS7 cells grown under steady-state conditions, all YPEL genes are expressed at varying levels (Figure 2c).

The experimental challenge was also evident when we attempted to detect the YPEL2 protein with commercially available and purportedly YPEL2-specific antibodies in WB or ICC studies in which we could not detect a YPEL protein using these YPEL2 antibodies (data not shown). However, we effectively observed the synthesis of 3F-YPEL2 and 3F-tagged YPEL proteins with ICC and WB using the Flag antibody in MCF7 or COS7 cells upon ectopic expressions. Of the antibodies we tested, a pan-YPEL antibody, which is an affinity-purified polyclonal antibody raised against a peptide that corresponds to an internal region of YPEL1, with amino acid sequences largely common within YPEL2, 3, and 4 of human origin (SCBT, S-14 Ypel antibody, sc99727),

detected YPEL1, 2, 3, and 4 but not YPEL5 in WB of COS7 cells (Figure 2d). Similarly, this antibody also detected, albeit at low levels, a protein species with electrophoretic mobility of about 13–14 kDa, likely corresponding to YPEL1, YPEL2, YPEL3 subtype1, and YPEL4 proteins of COS7 cells in WB (Figure 2e). This observation is supportive of a previous finding using an in-house pan-YPEL polyclonal antibody raised against a synthetic peptide corresponding to the carboxyl-terminal amino acid sequences of YPEL1-4 proteins that COS7 cells synthesize a YPEL protein(s) (Baker, 2003). The use of this in-house pan-YPEL antibody also suggested that YPEL(s) localizes to the nucleus and nucleus periphery, including the centrosomic region and nucleoli during interphase and around the mitotic apparatus during the mitotic phase of COS7 cells (Baker, 2003). Similarly, mouse Ypel1 as a GFP-fusion protein is reported to localize to the nucleus in transfected NIH3T3 mouse fibroblast cells (Roxström-Lindquist & Faye, 2001). Likewise, YPEL3 localization is suggested to be weakly nuclear with punctate perinuclear staining (Heminger et al., 2009). On the other hand, YPEL3, using a YPEL3-specific antibody, is reported to show diffuse staining, including nucleus and cytoplasm (Miller & Yelton, 2017). The pan-YPEL antibody we used to detect the Flag-YPEL proteins in WB analyses reveals staining in un-transfected COS7 cells encompassing both the cytoplasm and the nucleus as well as denser staining puncta at the nuclear periphery reminiscent of the centrosomic region (Baker, 2003) (Figure 2f). Similar locations were also observed in transfected COS7 cells synthesizing 3F-YPEL2 (Figure 2g,h) detected with the Flag (Figure 2g) or the pan-YPEL antibody (Figure 2h). Likewise, the GFP-3FYPEL2 fusion protein showed a diffuse intracellular location (Figure 2i).

The presence of a YPEL protein in COS7 cells suggests that YPEL protein(s) have functional roles in these cells. We, therefore, selected COS7 cells to assess YPEL2 functions. Although we were aware that co-expressions/co-syntheses of YPELs with functional commonalities could compensate for the effects of targeted downregulation of YPEL2, we nevertheless initially selected to use siRNA approaches to assess the role of YPEL2 in cellular processes. However, high sequence nucleotide homologies among YPEL transcripts (Figure S1) rendered the design of siRNAs with various tools to target specifically YPEL2, any or all members of the YPEL family, difficult. In several attempts with our design or commercially available siRNAs, we were unsuccessful in effectively altering the YPEL expressions in COS7 cells (data not shown). We, therefore, used an overexpression system to examine YPEL2 functions. We decided to use an inducible expression approach to circumvent possible adverse
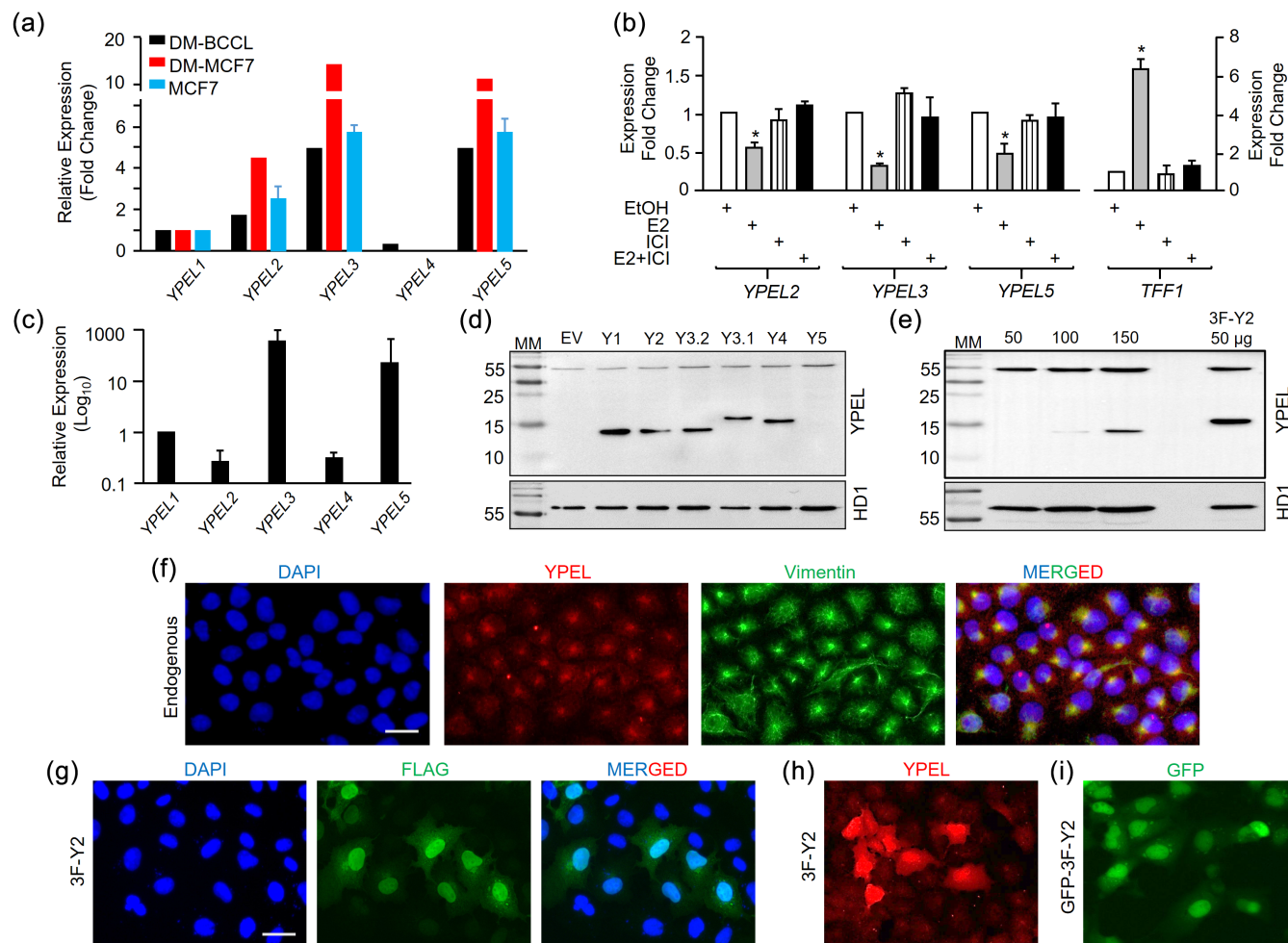
FIGURE 2 Expression of the YPEL family genes in cell lines. (a) Based on data from the DepMap portal, the average expression of the YPEL gene family members relative to the expression of *YPEL1* in breast cancer cell lines (DM-BCCL) or only in MCF7 cells (DM-MCF7) is shown. For comparison, our RT-qPCR analyses for the relative expression of YPEL genes in MCF7 cells (MCF7) are also indicated. (b) To assess whether or not E2-ERα signaling is involved in the regulation of *YPEL2, 3*, and *5* expressions, MCF7 cells grown for 72 h in CD-FBS containing growth medium were treated without (EtOH as control) or with 10^{-9}M E2, and/or 10^{-9}M ICI, a complete ER antagonist, for 24 h. cDNAs generated from total RNA were subjected to qPCR. We also used the E2-ERα responsive gene TFF1 as a control. Star indicates a significant change compared to EtOH control. (c) Relative to *YPEL1*, the expression of YPEL genes in COS7 cells was assessed by qPCR using cDNA from total RNA obtained from COS7 cells grown in steady-state conditions. (d) To evaluate the synthesis of YPEL1-5 proteins, which Y3.1 and Y3.2 indicate short and long variant YPEL3 proteins, COS7 cells were transiently transfected with the expression vector pcDNA3.1(−) bearing none (EV) or cDNA for a YPEL protein. Total protein extracts of COS7 cells grown in steady-state condition were subjected to SDS-15%PAGE followed by WB using a pan-YPEL antibody (SCBT, sc99727) and an HRP-conjugated goat-anti-rabbit secondary antibody (Advansta R-05072–500). Membranes were re-probed with an antibody specific to HDAC1 (Abcam, ab19845). Molecular masses (MM) in kDa are indicated. (e) To assess the synthesis of endogenous YPEL proteins in COS7 cells, protein extracts ranging from 50 to 150 μg were subjected to WB using the pan-YPEL antibody. We also used protein extracts from COS7 cells transiently transfected with pcDNA3.1(−) bearing the 3F-YPEL2 cDNA for comparison. Membranes were re-probed with the HDAC1 antibody (Abcam, ab19845). Molecular masses (MM) in kDa are indicated. (f) To assess the intracellular localization of endogenous YPEL (YPEL) proteins, COS7 cells grown on coverslips were subjected to ICC using the pan-YPEL antibody followed by an Alexa Fluor 594-conjugated goat anti-rabbit secondary antibody (Abcam, ab150080) or a vimentin (sc-6260) antibody followed by an Alexa Fluor 488-conjugated goat anti-mouse secondary antibody (Abcam, ab150113). DAPI was used to indicate the nucleus. The scale bar is 20 μm. (g,h) The intracellular localization of 3F-YPEL2 was evaluated in transiently transfected cells with the use of the Flag (g) or the pan-YPEL (h) antibody or GFP fusion (i). DAPI staining indicates the nucleus. The scale bar is 20 μm.

effects of YPEL2 overexpression on cellular phenotypes, as we observed acute cell death in MCF7 cells upon overexpression (data not shown). pINDUCER20 is a tightly controlled tetracycline-inducible lentiviral single-vector that provides a constitutive expression of the reverse tetracycline transactivator 3 (rtTA3) and contains promoter
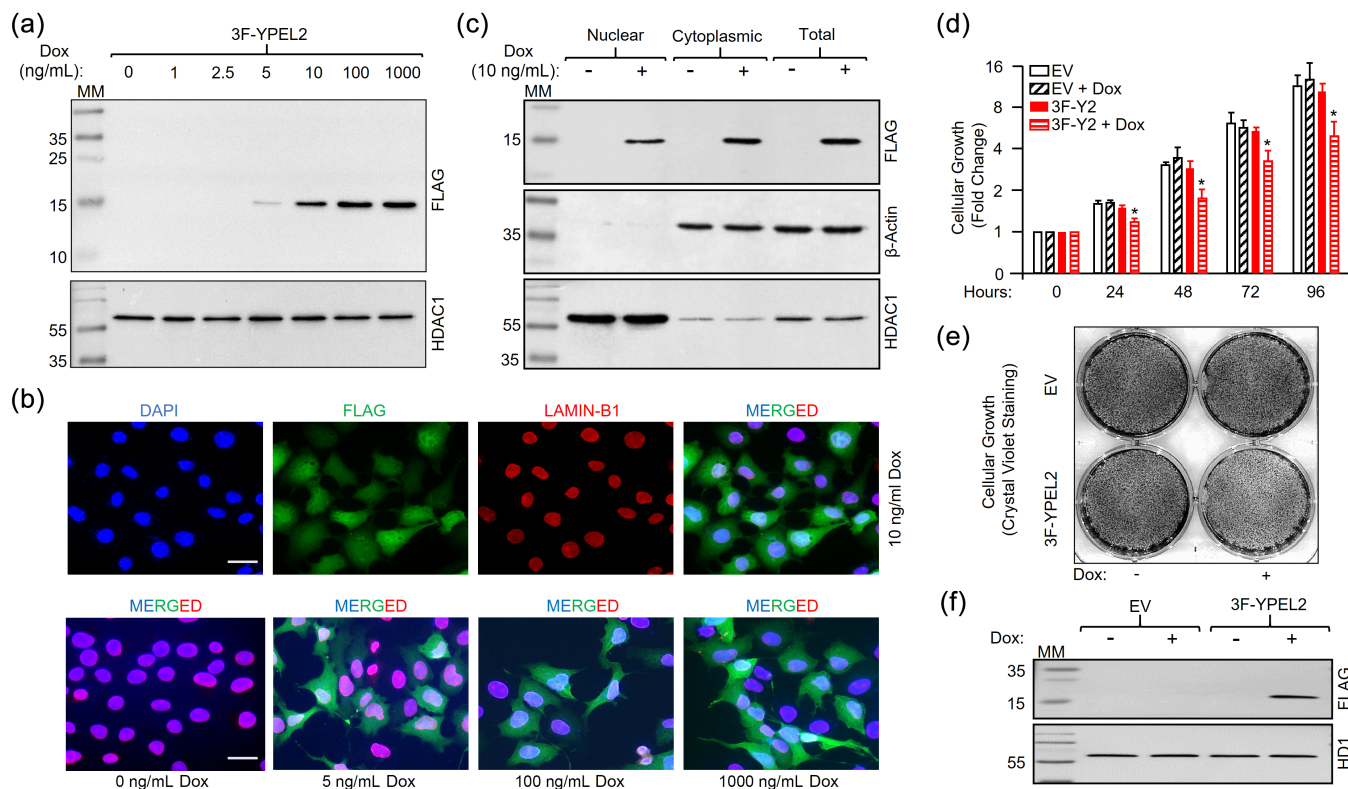
FIGURE 3 Assessing effects of 3F-YPEL2 on the growth of COS7 cells. (a) COS7 cells were transiently transfected with the pINDUCER20-MCS vector bearing none (EV) or the 3F-YPEL2 cDNA for 24 h. Cells were treated without (0) or with varying concentrations (1–1000 ng/mL) of Dox for 24 h. Total cell extracts (50 μg) were then subjected to WB using the Flag antibody followed by an HRP-conjugated goat-anti-mouse secondary antibody (Advansta R-05071-500). Membranes were re-probed with the HDAC1 antibody. Molecular masses (MM) in kDa are indicated. (b) Transiently transfected cells with pINDUCER20-MCS bearing the 3F-YPEL2 cDNA for 24 h were then treated with 0, 5, 10, or 100 ng/mL Dox for 24 h. Cells were subsequently fixed, permeabilized, washed, and stained with the Flag antibody, followed by an Alexa Fluor 488-conjugated goat anti-mouse secondary antibody (Abcam, ab150113) or a Lamin B1 antibody (Abcam, ab16048), followed by an Alexa Fluor 647-conjugated goat anti-rabbit secondary antibody. DAPI was used to indicate the nucleus. The scale bar is 20 μm. (c) To assess the subcellular levels of inducibly synthesized 3F-YPEL2 in transiently transfected cells treated without or with various concentrations of Dox for 24 h, fractionated nuclear and cytoplasmic protein extracts were subjected to WB using the Flag antibody. Membranes were re-probed with an antibody specific to β-actin (Abcam, ab8227) or HDAC1 (Abcam, ab19845). Molecular masses (MM) in kDa are indicated. (d) To assess the effects of 3F-YPEL2 on cellular growth, COS7 cells transiently transfected with pINDUCER20-MCS bearing none (EV) or the 3F-YPEL2 cDNA for 24 h were treated without or with 10 ng/mL Dox for 24 h intervals up to 96 h. At every 24 h, cells were collected and counted with a hematocytometer. The asterisk indicates significant changes ($p < 0.05$) in cellular growth depicted as fold changes. (e) Crystal violet staining for cellular growth and (f) WB analysis with the Flag antibody of COS7 cells inducibly synthesizing 3F-YPEL2 at 96 h are shown.

sequences composed of tetracycline-responsive elements (TRE) for transgene expression (Baek et al., 2021). The constitutively synthesized rtTA3 induces transgene expression from the TRE-driven promoter upon binding to tetracycline or its stable analog Dox (Baek et al., 2021). We inserted the 3F-YPEL2 cDNA with appropriate restriction sites into pINDUCER20-MCS, which we modified by inserting a multiple cloning site (MCS) to ease transgene cloning. We then transiently transfected COS7 cells with pINDUCER20-MCS bearing none or the 3F-YPEL2 cDNA. We observed by WB and ICC that Dox effectively induced 3F-YPEL2 synthesis, the levels of which were correlated with Dox concentrations: The minimal amount of Dox required for the maximal amount of 3F-YPEL2 synthesis was 10 ng/mL (Figure 3a). Independent of Dox concentrations, 3F-YPEL2 showed diffuse intracellular staining, as we observed with the endogenous YPEL1-4 proteins (Figure 2f), including the nucleus and cytoplasm (Figure 3b) which we further confirmed with WB using fractionated cellular proteins (Figure 3c).

Since the YPEL family proteins appear to be involved in alterations of cellular phenotype, we initially assessed the effect of YPEL2 on cellular proliferation in COS7 cells

transfected with pINDUCER20-MCS bearing none or the 3F-YPEL2 cDNA for 24 h. Cells were treated without or with 10 ng/mL Dox for up to 96 h with fresh medium every 24 h. We found by cell counting (Figure 3d) and crystal violet staining, which is shown at 96 h (Figure 3e), that 10 ng/mL Dox-induced 3F-YPEL2 synthesis reduces cellular proliferation (Figure 3f). Interestingly, the decline in cellular proliferation appeared to occur only at 24 h Dox treatment without altering the rate of proliferation at subsequent time points which remained the same throughout (Figure 3d) even though cell synthesized 3F-YPEL2 at levels that were similar at all time points (Figure S3a). However, we could not ascertain how 3F-YPEL2 synthesis led to the repression in cell growth at 24 h, at which we observed no significant changes in cell cycle distribution assessed with flow cytometry (Figure S3b) or in cell death by Annexin V staining (Figure S3c).

2.1 | Dynamic analyses of proximity protein interaction network of YPEL2

Although YPEL2 appears to be involved in processes culminating in cellular proliferation, the underlying mechanism is unclear. Since proteins function within protein interaction networks which are critical for cellular processes, we reasoned that the identification of interacting partners of YPEL2 in a time-dependent manner could provide crucial information about YPEL2 functions. To explore this issue, we used the TurboID proximity labeling approach, which is a derivative of the BioID system (Meerbrey et al., 2011; Roux et al., 2012), which we previously utilized (Roux et al., 2018). TurboID uses a biotin ligase engineered through yeast display-based directed evolution of a promiscuous mutant of *E. coli* biotin ligase BirA* that catalyzes proximity biotin labeling of proteins with higher efficiencies and faster kinetics than BirA*. This allows the investigation of protein interaction networks dynamically (Ayaz et al., 2021). Based on our initial analyses that TurboID can be effectively used for dynamic protein interaction profiling of YPEL2 (Figure S4), we cloned the Turbo-HA, 3F-YPEL2, or 3F-YPEL2-Turbo-HA cDNA into pINDUCER20-MCS to efficiently dictate the timing and the level of protein synthesis in transiently transfected cells to minimize potential adverse effects of transgene overexpression. We transiently transfected COS7 cells with the expression vectors for 24 h. Cells were treated with 10 ng/mL Dox for 24 h to induce 3F-YPEL2 synthesis. We then treated cells with 50 μM biotin and 1 mM ATP for 1, 3, 6, or 16 h in the presence of 10 ng/mL Dox followed by WB

(Figure 4a,b) and ICC (Figure 4c) using an antibody specific for the Flag, HA, or biotin. Results, shown are biotin labeling for 3 h, revealed that cells only in the presence of Dox synthesize 3F-YPEL2, Turbo-HA, or 3F-YPEL2--TurboID-HA with an expected MM of approximately 17, 37, or 54 kDa protein respectively (Figure 4a). The proteins show diffuse intracellular staining encompassing both the nucleus and cytoplasm independently of the exogenously added biotin (Figure 4c). Importantly, the detection of many biotinylated proteins only in the presence of biotin in transfected cells synthesizing 3F-YPEL2-TurboID-HA indicates that the fusion protein is functional as well. The detection of Turbo-HA or 3F-YPEL2-TurboID-HA with the Biotin antibody in the absence of exogenously added biotin also suggests self-labeling of the proteins with residual endogenous biotin (Figure 4a).

Based on these results and our preliminary studies (Figures S4 and S5), we carried out large-scale biotin labeling of intracellular protein for MS analyses. COS7 cells transiently transfected with pINDUCER20-MCS bearing (i) none (EV), (ii) the Turbo-HA, or (iii) the 3F-YPEL2-Turbo-HA cDNA for 24 h were subjected to 10 ng/mL Dox for 24 h. Cells were then incubated in a fresh medium containing 50 μM biotin and 1 mM ATP for 1, 3, 6, and 16 h. Cells were lysed, and biotinylated proteins in cell lysates were captured with streptavidin-conjugated magnetic beads. After on-bead tryptic proteolysis of the captured proteins, protein fragments were subjected to MS analyses. MS identified many proteins from each group conducted as two biological replicates. Subtractive analyses of identified proteins generated from cells transfected with (i) none (UT), (ii) pINDUCER20-MCS bearing the Turbo-HA, or (iii) pINDUCER20-MCS bearing the 3F-YPEL2-Turbo-HA cDNA revealed 130, 99, 157, and 115 specific proximal interactors of YPEL2 at 1, 3, 6, and 16 h respectively (Data S1: proximity interactors). We found that many proteins were present only at a distinct time point; some were common at specific or all time points examined (Figure 5a,b).

It should be noted that of the previously identified proteins STRN as a YPEL1 interacting protein (Branon et al., 2018); SH2D4A (Huttlin et al., 2017) and SRPK2 (Luck et al., 2020) as YPEL2 interactors; LARP4, SH2D4A, SPG21, SRPK2, TP53, and TRIP6 as YPEL3 interacting partners (Huttlin et al., 2017); DDX5 (Varjosalo et al., 2013), ELAVL1 (Boldt et al., 2016) LARP4 (Abdelmohsen et al., 2009), PFDN5 (Huttlin et al., 2017), and RANBP9 (Hosono et al., 2004; Varjosalo et al., 2013) as YPEL5 interacting proteins are also present in our protein interaction network of YPEL2. This
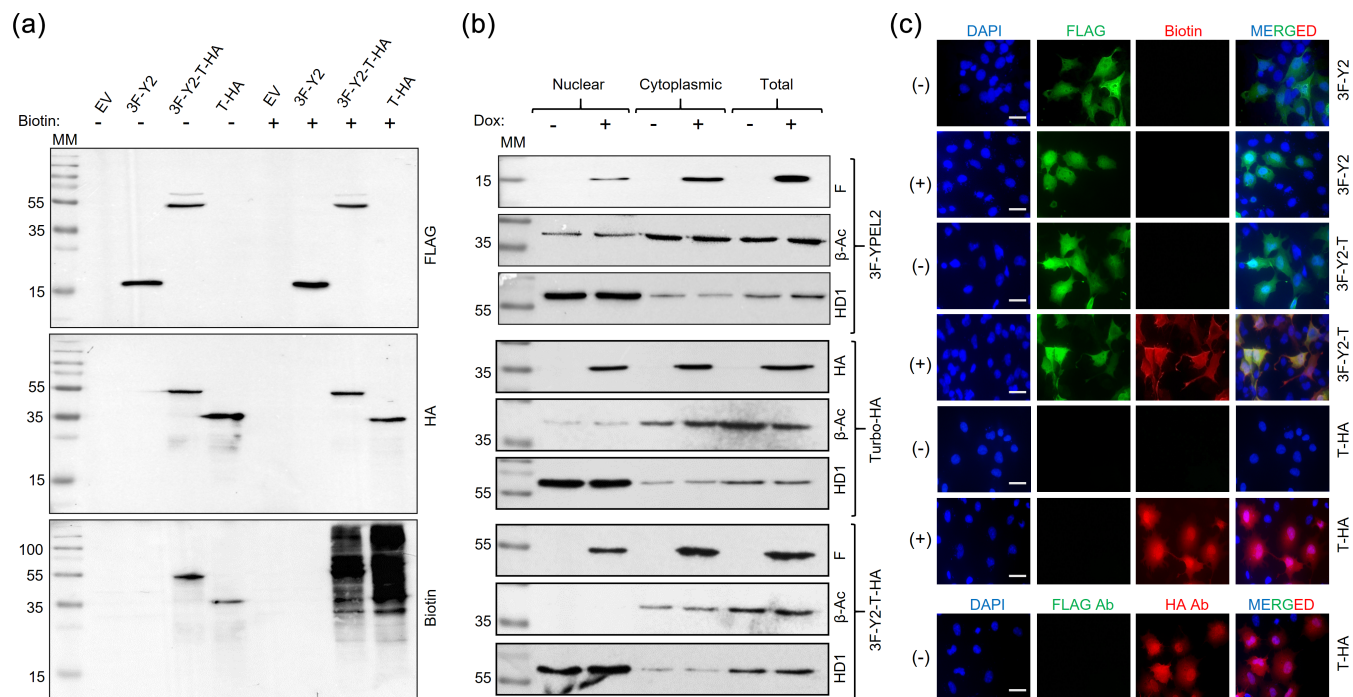
FIGURE 4 Synthesis, subcellular location, and effects of TurboID constructs on the biotinylation of intracellular proteins in COS7 cells. (a) COS7 cells were transfected with pINDUCER20-MCS carrying none (EV), the 3F-YPEL2 (3F-Y2), 3F-YPEL2-Turbo-HA (3F-Y2-T-HA), or Turbo-HA (T-HA) cDNA. Twenty four hours after transfection, cells were treated without or with 10 ng/mL Dox to induce protein synthesis for 24 h in the absence or presence of biotin (50 μM) for the biotinylation of endogenous proteins. Cells were then collected, and equal amounts (50 μg) of protein extracts were subjected to SDS-10%PAGE electrophoresis followed by WB analyses using the Flag, HA, or Biotin (Abcam, ab53494) antibody. Molecular masses are indicated in kDa. (b) To assess subcellular distributions of 3F-YPEL2 (3F-Y2), Turbo-HA (T-HA), or 3F-YPEL2-Turbo-HA (3F-Y2-T-HA) proteins following 10 ng/mL Dox induction for 24 h in transiently transfected cells, cytoplasmic, nuclear, or the total protein extracts (50 μg) were subjected to WB analyses wherein β-actin (β-Ac, ab8227) and HDAC1 (HD1) were used as the cytoplasmic and nuclear protein loading controls. Molecular masses are depicted in kDa. (c) Intracellular locations of the TurboID constructs in the transiently transfected cell grown on coverslips without (−) with Biotin (+) were assessed with the Flag antibody followed by the Alexa Fluor 488-conjugated secondary antibody (Abcam, ab150113), or HA and/or biotin antibody followed by the Alexa Fluor 594-conjugated secondary antibody (Abcam, ab150080). DAPI staining indicates the nucleus. The scale bar is 20 μm.

observation suggests that YPEL2 and other YPEL proteins function similarly.

To assess ontologies of putative interacting proteins of YPEL2 for biological functions, we analyzed the MS results with the Metascape portal (https://metascape.org/), which is an integrated web-based system that allows functional enrichment, interactome analysis, gene annotation, and membership search (Youn et al., 2018). Results revealed that the profile of proximity interaction partners of YPEL2 changes dynamically generating a temporal enrichment of Gene Ontology (GO; http://geneontology.org/) and Reactome pathway (https://reactome.org/) terms (Figure 5c). We find common enrichment of proteins at all time points in GO and Reactome terms that encompass RNA and mRNA metabolic processes, ribonucleoprotein complex biogenesis, regulation of gene silencing by miRNA, and cellular responses to stress, Proximity interaction partners of YPEL2 involved in RNA metabolic processes include

CELF1, DDX6, DDX52, EEF1D, EIF4H, ELAVL1, G3BP1, HSPA8, HNRNPA0, HNRNPDL, LARP4B, PTBP1, SMN1, SQSTM1, and UPF1 and proteins subgrouped in cellular responses to stress include AGO2, ANAPC, PN1, BAG3, GFPT1, HSP90B1, MAP4K4, RPS, STAT3, TNRC6A, TP53, and TUBB4B. GO-terms also include common proteins at secondary neighbor levels. For example, HSPA8, TNRC6A, and TNRC6B as proximity interactors of YPEL2 proteins involved in RNA metabolic processes are also found to be associated with the GO-term clustering of "cellular stress response" as secondary neighbors that contain a large group of proteins exemplified with AGO1, EXOSC2, and NUP98. Similarly, RPS25 and RPLP0 sub-grouped in the GO-term of "cellular response to stress" show functional associations with proteins enriched in the GO-term of "ribonucleoprotein complex biogenesis," including AGO1, AGO3, and RPL10 as secondary neighbors (Figure S6 and Data S2: secondary neighbors).

FIGURE 5 In silico analysis of proximal interaction partners of YPEL2. (a) Intersections of proximal protein partners of YPEL2 at different time points were constructed using a Venn diagram tool (https://bioinformatics.psb.ugent.be/webtools/Venn/). (b) The Circos plot generated with Metascape indicates time-dependent (outside arcs with distinct colors for each time point) proximal interaction partners of YPEL2 that are shared among time points (inside arcs with a dark orange color linked with purple lines). (c) A hierarchically clustered heatmap of enriched terms related to functions of proteins across all time points colored by p-values was generated by Metascape.

Furthermore, and importantly, the identities of a substantial number of the putative protein partners of YPEL2 at all time points appear to be coincident with proteins involved in the formation of processing bodies (p-bodies, PBs), and stress granules (SGs) (Zhou et al., 2019) as cytoplasmic ribonucleoprotein (RNP)

assemblies (Figure 6a,b). These include canonical markers of PBs including AGO2, DCP1A, EDC3, and TNRC6A, markers of SGs comprising ATXN2, ELAVL1, G3BP1, NCOA3, PABPC1, SQSTM1, TARDBP, and USP10 proteins as well as proteins shared between SGs and PBs including AGO2, DDX2, XRN1 (Abdelmohsen et al., 2009; Millar et al., 2022; Wheeler et al., 2016; Zhou et al., 2019).

Our findings that the putative YPEL2 partners include proteins involved in RNA metabolic processing, in the formation and/or sustaining PBs and SGs, together with the network analyses of all-time points with Metascape (Figure 6c,d), imply the involvement of YPEL2 in responses to stress under both steady-state and stress conditions.

## 2.2 | Assessing the interaction of YPEL2 with putative protein partners

Based on functional importance derived from our Metascape analyses, we selected ADSS, EEF1D, ELAVL1, G3BP1, and SQSTM1 for the initial interaction screening to test whether or not they are protein partners of YPEL2. ADSS (Adenylosuccinate synthetase-1 and -2 with estimated MMs of 50.2 and 50.09 kDa, respectively) plays a critical role in the de novo and the salvage pathway of purine nucleotide biosynthesis by carrying out initial steps in the biosynthesis of adenosine monophosphate (AMP) from inosine monophosphate (Hubstenberger et al., 2017). Eukaryotic translation elongation factor 1 delta (EEF1D) with a predicted MM of 71.4 kDa is a subunit of the elongation factor-1 complex and functions as a guanine nucleotide exchange factor by stimulating the exchange of GDP to GTP in EEF1A1 (Dewulf et al., 2022). ELAV like RNA binding protein 1 (ELAVL1), an RNA-binding protein (RBP) with an estimated 36 kDa MM, binds to poly-U and AU-rich elements (AREs) in the 3′-UTR of target mRNAs and increases their stability (Ma et al., 1996; H. Xu et al., 2021). ELAVL1 is also involved in SG maturation (Ma et al., 1996; H. Xu et al., 2021). G3BP stress granule assembly factor 1 (G3BP1), with an estimated MM of 52 kDa, is an RBP and a key component of SG assembly (Kedersha et al., 2016; Wu & Xu, 2022). Localized also in SGs, SQSTM1 (Sequestosome-1) with an MM of 47.7 kDa is an autophagy receptor required for selective macro-autophagy by functioning as a bridge between polyubiquitinated cargo and autophagosomes (Lamark et al., 2017; Protter & Parker, 2016). To validate the interaction between YPEL2 and a putative interacting partner, we transiently transfected COS7 cells with the expression vector pcDNA3.1(−) bearing none, 3F-YPEL2 and/or HA-ADSS, HA-EEF1D, HA-ELAVL1, HA-G3BP1 or HA-SQSTM1 cDNA for 48 h. Our preliminary Co-IP studies did not detect an interaction between 3F-YPEL2 and HA-ADSS, HA-EEF1D, or HA-G3BP1 (Figure S7). We found, on the other hand, that 3F-YPEL2 interacts with HA-ELAVL1 (Figure 7a–d) or HA-SQSTM1 (Figure 7e–h).

Based on these results, we further characterized the interaction of YPEL2 with ELAVL1 or SQSTM1. In transiently transfected COS7 cells with expression vectors bearing the 3F-YPEL2 and/or HA-ELAVL1 cDNA, YPEL2 alone shows diffuse staining encompassing both the nucleus and cytoplasm (Figure 7a). Although HA-ELAVL1 localizes primarily to the nucleus (Kageyama et al., 2021), we also observe the localization of HA-ELAVL1 in the cytoplasm with intensely stained cytoplasmic foci wherein the 3F-YPEL2 staining shows overlaps. This observation suggests that ELAVL1 and YPEL2 co-localize to cytoplasmic structures, reminiscing of PGs/SGs. HA-ELAVL1 in transfected cells shows discrete electrophoretic migration with an MM of about 37 kDa, whereas 3F-YPEL2 displays an electrophoretic species migrating at 17 kDa MM (Figure 7b). Immunoprecipitation of cellular extracts of transiently transfected cells that co-synthesize 3F-YPEL2 and HA-ELAVL1 using the HA or the Flag antibody together with protein A and G magnetic beads followed by immunoblotting with the Flag or the HA antibody indicates the presence of both HA-ELAVL1 and 3F-YPEL2 in the mmunoprecipitated samples (Figure 7c). The co-localization or Co-IP results were not due to the nature of the tags as we observed 3F-ELAVL1 and HA-YPEL2 interact and co-localize to PGs/SGs-like structures when co-synthesized (Figure S8) These results demonstrate that 3F-YPEL2 and ELAVL1 interact only in the cytoplasm.

To further verify that ELAVL1 is an interacting protein partner of YPEL2, we carried out the proximity ligation assay (PLA) as we described previously (Roux et al., 2018). PLA utilizes species-specific secondary antibodies conjugated with distinct DNA primers. A hybridization step followed by circular DNA amplification with fluorescent probes to the conjugated DNA primers allows the visualization of proximity spots by fluorescence microscopy (Doller et al., 2008). In transiently transfected COS7 cells, we observed prominent fluorescence signals in the cytoplasm only when cells co-synthesize HA-ELAVL1 and 3F-YPEL2 in the presence of both the HA and the Flag antibodies (Figure 7d), as we observe virtually no fluorescence signal in the presence of a single antibody even when cells synthesize both interacting partners (Figure S9). These results support the conclusion that ELAVL1 is an interacting partner of YPEL2 when both proteins are present in the cytoplasm. Since

FIGURE 6 Cumulative network analysis of proximal interaction partners of YPEL2 at all points. (a and b) Intersections of proximal protein partners of YPEL2 at different time points with proteins of (a) processing bodies (Hubstenberger et al., 2017), PBs, or (b) stress granules (Millar et al., 2022), SGs, curated in the RNAgranuleDB database, version 2.0, Gold Standart (http://rnagranuledb.lunenfeld.ca/) were generated using a Venn diagram tool. (c) A network of enriched terms using all proximal interaction partners of YPEL2 is generated with Metascape and visualized with Cytoscape. A circle node where size is proportional to the number of proteins specific to a term is colored represented. Nodes that share the same cluster identity are represented close to each other. (d) The enriched term network is represented by colored *p*-values, where terms containing more proteins indicate more significant *p*-values.
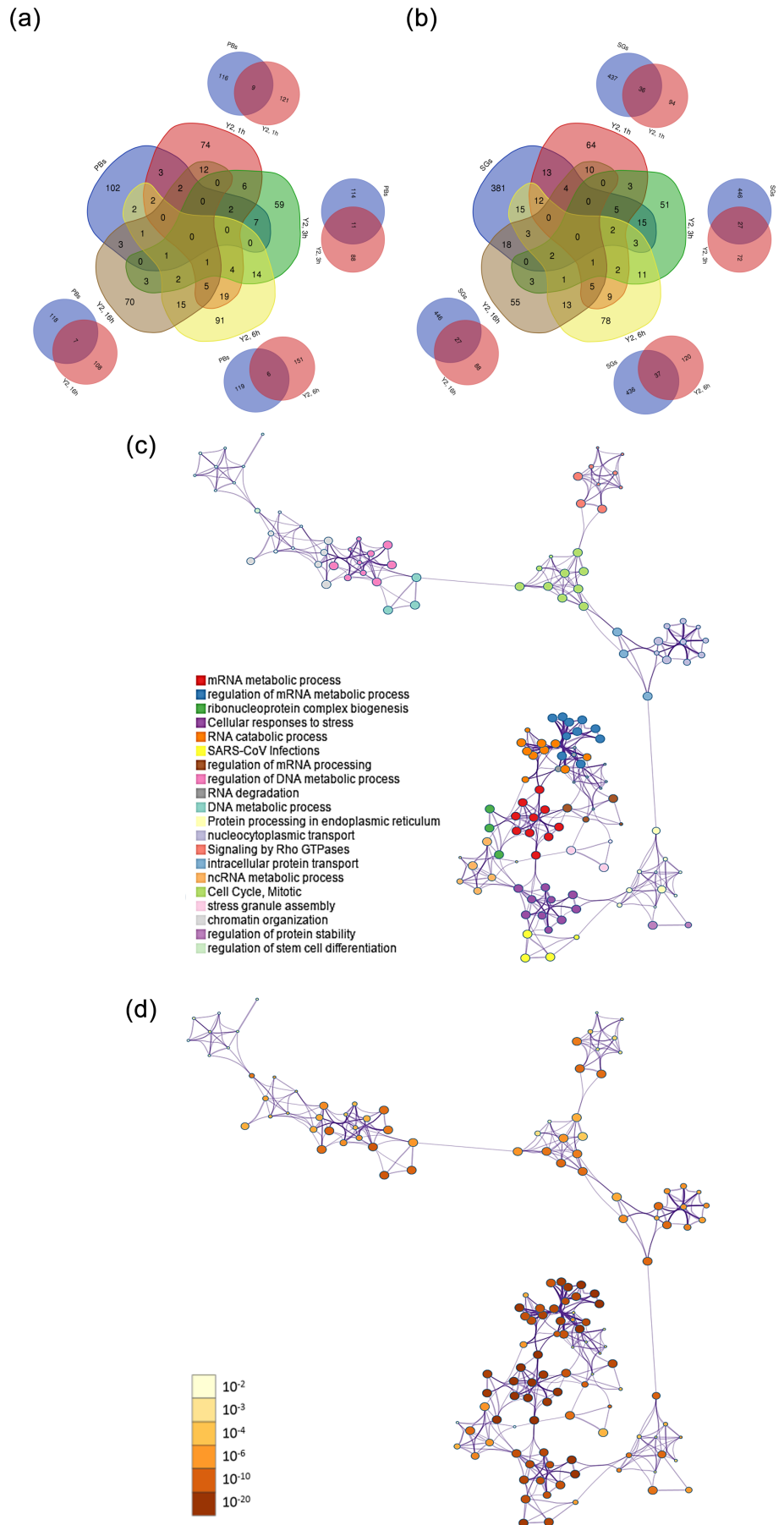
ELAVL1 is predominantly found in the nucleus but can translocate to the cytoplasm through phosphorylation of residues located in the hinge region of the protein (Kageyama et al., 2021), our results also imply that YPEL2 may interact with the phosphorylated ELAVL1.

Similar studies by the use of IP, WB, ICC, and PLA in transient transfection into COS7 cells with expression vectors bearing the 3F-YPEL2 and/or HA-SQSTM1 cDNA indicated that SQSTM1 is also an interaction partner of YPEL2 (Figure 7e–h).
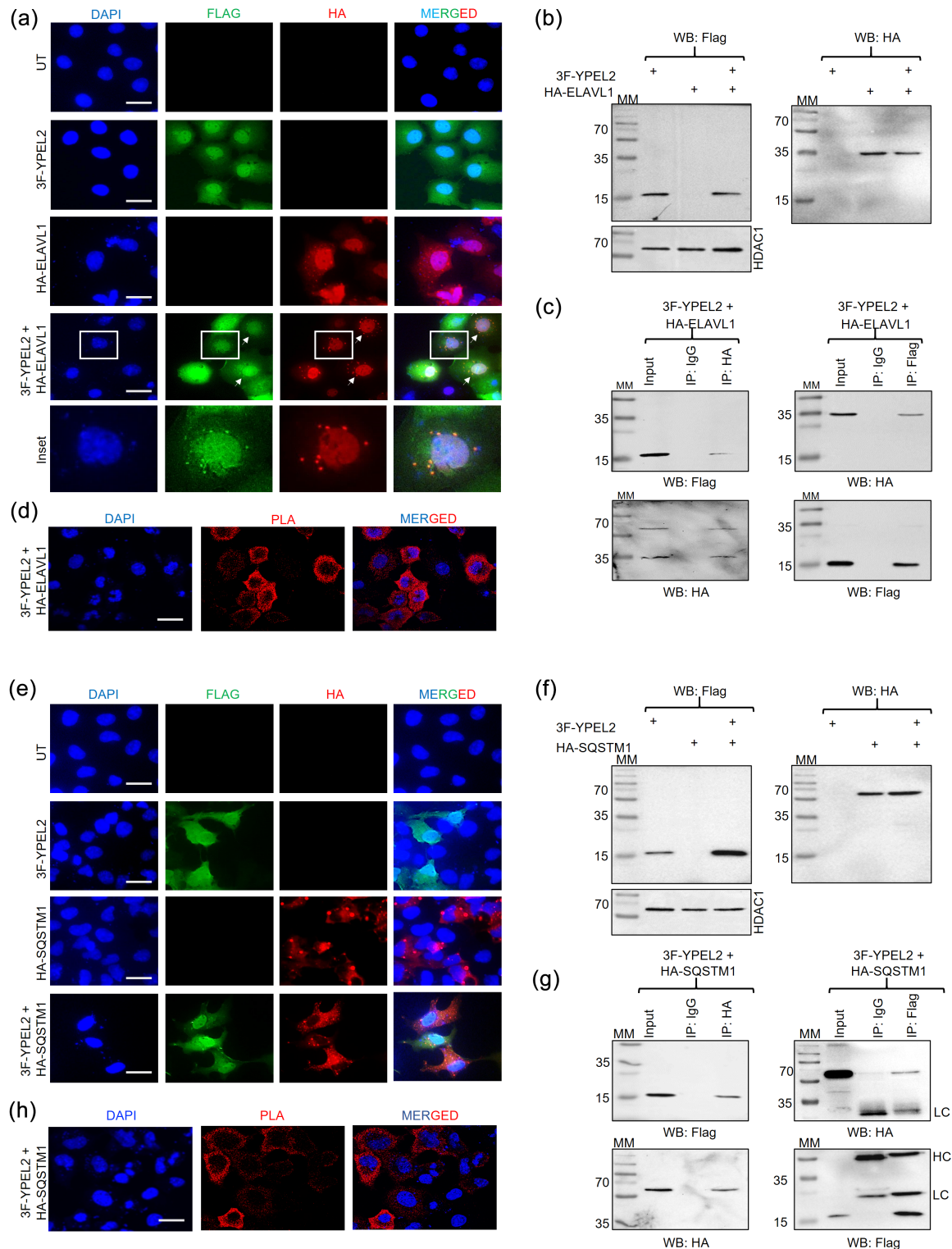

FIGURE 7 Legend on next page.

2.3 | Localization of the endogenous YPEL proteins in SG in response to SA

Interaction of YPEL2 with ELAVL1, or SQSTM1, and co-localizations in PB/SG-like structures in the cytoplasm suggest that YPEL2 is involved in processes associated with the formation and/or maintenance of PBs/SGs, thereby cellular stress responses. Because overexpression in experimental systems could induce SG formation without stress stimuli (Söderberg et al., 2008; Tourrière et al., 2001), to ensure that our results are not experimental artifacts, we examined the involvement of the endogenous YPEL in SG formation in cellular responses to a stress inducer. Since cells respond to various internal and external stresses, including heat shock, amino acid deprivation, hypoxia, and oxidative stress by inducing the formation of SGs[63] and since our Phyre2 results assign possible RNA binding and oxidoreductase activities to YPEL proteins (Figure 1c), we chose SA as an oxidative stress inducer to investigate SG formation (Colombrita et al., 2009; Liu-Yesucevitz et al., 2010; Matsuki et al., 2013; Millar et al., 2022).

To assess SG formation in COS7 cells in response to SA, we treated cells without (− SA) or with 200 μM SA (+ SA), which was based on the minimal concentration of SA to induce SG-like loci in all cells in 1 h (Figure S10). Cells were then subjected to RNA-FISH with an ATTO488-conjugated oligo-$(dT)_{50}$ probe for mRNA detection and/or RNA-FISH coupled ICC using a rabbit polyclonal antibody specific to G3BP1 as an essential nucleator of SG assembly to ensure that SA treatment of COS7 cells faithfully reconstitutes SG formation. We observed that oligo-$(dT)_{50}$ and G3BP1 signals merge to cytoplasmic foci only in response to SA, indicating that SA-induced cytoplasmic foci are bona fide SGs (Figure 8a). Under identical conditions, co-localization of endogenous YPEL, assessed with the pan-YPEL antibody, with G3BP1 probed with a mouse monoclonal antibody

specific to G3BP1 indicated that the endogenous YPEL proteins (YPEL) also localize to SGs (Figure 8b). In transiently transfected COS7 cells, co-localization of 3F-YPEL2 (assessed with the Flag antibody) with the endogenous G3BP1 in cytoplasmic foci in response to 200 μM SA shows that 3F-YPEL2 as the endogenous YPEL is present in SGs as well (Figure 8c).

SG assembly and disassembly occur dynamically through sequential multistep processes that involve an initial nucleation event, which follows a growth phase requiring the accumulation of substrate molecules and, finally, the fusion of the small initial stress granules into larger assemblies (Millar et al., 2022). To examine whether or not the endogenous YPEL is also involved in dynamic SG assembly and/or disassembly of SGs, we treated COS7 cells with 200 μM SA for 15-min intervals up to 2 h. Cells were then probed with the pan-YPEL and G3BP1 antibodies (Figure 8d). Results revealed that 15 min after SA treatment, the endogenous YPEL and G3BP1 co-localized to numerous and various sizes SGs. These SGs merged to form larger SGs, thereby decreasing the number of SGs at later times up to 2 h, within which YPEL and G3BP1 co-localized. Following a 1 h SA treatment (post-SA, PS, treatment), SGs completely disappeared within 4 h of the SA withdrawal, leading to diffuse staining of both YPEL and G3BP1 (Figure 8e). These results suggest that the YPEL proteins are indeed present in stress granules.

HA-G3BP1 did not interact (Figure S7) but co-localized with 3F-YPEL2 in SG-like structures in the cytoplasm of transiently transfected COS7 cells (Figure 8c). On the other hand, HA-ELAVL1 interacted and co-localized with 3F-YPEL2 in SG-like structures (Figure 7). This raises the possibility that the interaction between ELAVL1 and YPEL2 is critical for the localization of the endogenous YPEL in SGs. To examine whether or not reducing levels of the endogenous ELAVL1 protein decreases/represses the localization of

FIGURE 7 Interaction of 3F-YPEL2 and HA-ELAVL1. (a) To assess the intracellular localization of 3F-YPEL2 and/or HA-ELAVL1, COS7 cells grown on coverslips un-transfected (UT) or transiently transfected for 36 h with the expression vector pcDNA3.1(−) bearing the 3F-YPEL2 or HA-ELAVL1 cDNA were stained with the Flag or the HA antibody. DAPI was used to indicate the nucleus. The scale bar is 20 μm. (b) COS7 cells were transfected (+) with the expression vector bearing 3F-YPEL2 and/or HA-ELAVL1 cDNA to examine the protein synthesis. The synthesis of proteins was assessed by WB using the Flag or the HA antibody. HDAC1, used as a loading control, was probed with the HDAC1 antibody. (c) The cellular extracts (500 μg) of transiently co-transfected COS7 cells were subjected to Co-IP with the HA, Flag, or isotype-matched IgG. Fifty micrograms of lysates was used as input control. The precipitates were subjected to SDS-10%PAGE followed by WB using the Flag or the HA antibody. Molecular masses (MM) in kDa are indicated. (d) To assess *in cellula* interaction of 3F-YPEL2 and HA-ELAVL1, the proximity ligation assay was carried out in transiently transfected COS7 cells grown on coverslips. Cells were fixed, permeabilized, blocked, and probed with the HA and/or the Flag antibody. Cells were then subjected to fluorescent probes for circular DNA amplification for proximity interaction foci. DAPI was used for nuclear staining. Images were captured with a fluorescence microscope. The scale bar is 20 μm. (e) The intracellular localization, (f) protein synthesis, (g) interaction, and (h) PLA of 3F-YPEL2 and/or HA-SQSTM1 in transiently transfected COS7 cells were assessed as described in the legend of a–d. HDAC1 was used as a loading control.
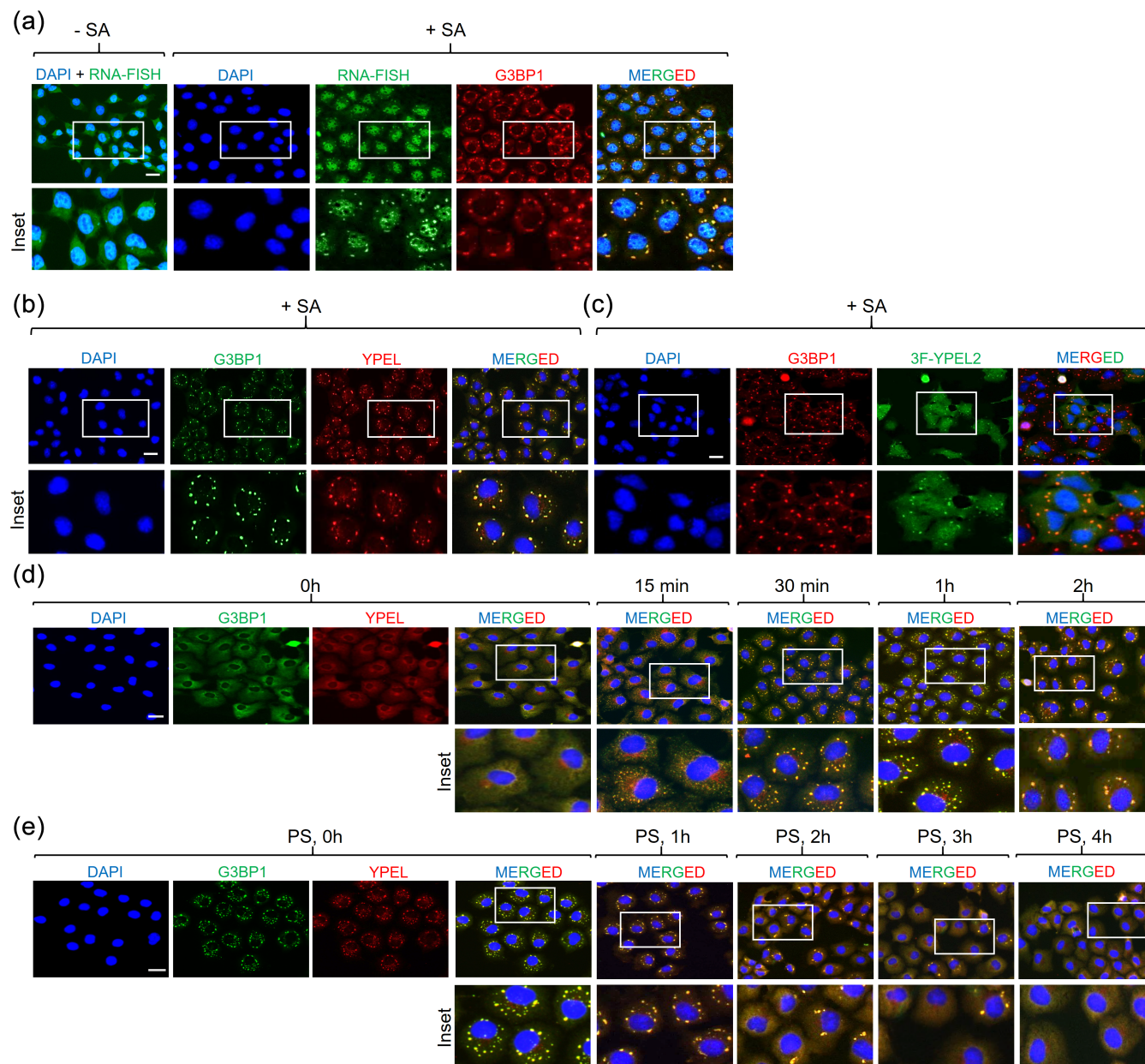
FIGURE 8 Stress granule formation in COS7 cells in response to sodium arsenite (SA). (a) To assess the formation of stress granules, COS7 cells grown on coverslips were treated without (−SA) or with 200 μM sodium arsenite (+SA) for 1 h. Cells were fixed and subjected to hybridization-couple ICC using an ATTO488 conjugated oligo-dT probe and the polyclonal G3BP1 antibody (ab200550) followed by an Alexa Fluor-647 conjugated secondary antibody. DAPI indicates the nucleus. The scale bar is 20 μm. (b) To assess the co-localization of the endogenous YPEL proteins (YPEL) with G3BP1, cells treated with SA for 1 h were fixed and subjected to ICC using the monoclonal G3BP1 antibody (SCBT, sc-365338) followed by an Alexa Fluor-488 conjugated secondary antibody (405319, Biolegend) and the pan-YPEL antibody (SCBT, sc99727) followed by an Alexa Fluor-647 conjugated goat-rabbit secondary antibody (Abcam, ab150083). DAPI was used to indicate the nucleus. (c) To assess whether 3F-YPEL2 also co-localizes with G3BP1 in SGs, cells transfected with the expression vector pcDNA3.1(−) bearing 3F-YPEL2 cDNA were subjected to ICC using the polyclonal G3BP1 antibody (Abcam, ab200550) followed by an Alexa Fluor-647 conjugated secondary antibody and the monoclonal Flag antibody (Sigma-Aldrich, F1804) followed by an Alexa Fluor 488-conjugated secondary antibody. DAPI indicates the nucleus. (d) To examine the co-localization of YPEL and G3BP1 during the formation and disassembly of SGs, COS7 cells grown on coverslips were treated with 200 μM sodium arsenite (+SA) for 0, 15 min, 30 min 1 h, and 2 h. (e) Following 1 h of 200 μM sodium arsenite (+SA) treatment, cells (post-stress, PS) were washed and incubated in the growth medium without SA for 0, 1, 2, 3, or 4 h. (d and e) Fixed cells were then subjected to ICC using the monoclonal G3BP1 antibody (sc-365338) and the pan-YPEL antibody (sc99727) followed by secondary antibodies for visualization with a fluorescence microscope. DAPI staining indicates the nucleus. The scale bar is 20 μm.
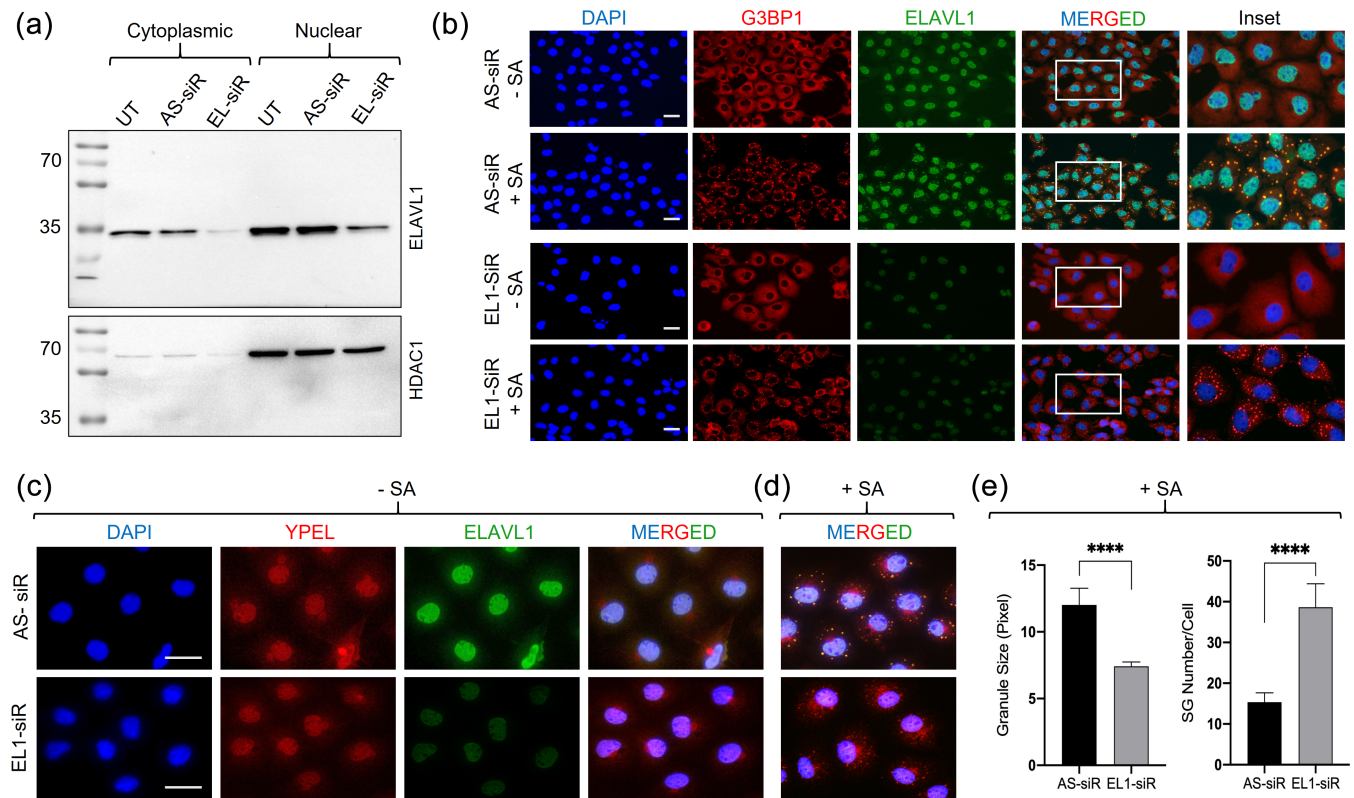
FIGURE 9 Effects of suppressed levels of ELAVL1 by a siRNA approach on the co-localization of YPEL and G3BP1 in SGs. (a) To examine whether or not a reduction of ELAVL1 levels in cells alters the location of YPEL in SGs, COS7 cells were left un-transfected (UT) or transiently transfected with a control siRNA AllStar (AS-siR) or a siRNA pool specific to ELAVL1 transcripts (EL-siR) for 24 h. Cytoplasmic and nuclear extracts (50 µg) were subjected to SDS-10%PAGE for WB analysis using a monoclonal antibody specific to ELAVL1 (SCBT, sc-5261). HDAC1 probed with the HDAC1-specific antibody (Abcam, ab19845) was used as the loading control. (b) Transfected COS7 cells with the AllStar siRNA or the ELAVL1 siRNA pool for 24 h were also treated without (−SA) or with 200 µM sodium arsenite (+SA) for 1 h. Cells were then fixed and subjected to ICC using the ELAVL1 antibody or the pan-YPEL antibody. DAPI staining indicates the nucleus. The scale bar is 20 µm. (c and d) To assess the co-localization of ELAVL1 and YPEL in SGs when ELAVL1 protein levels were reduced, COS7 cells transfected with (c) the control (AS-siR) or with (d) the siRNA pool specific to ELAVL1 transcripts (EL-siR) for 24 h were treated without (−SA) or with 200 µM sodium arsenite (+SA) for 1 h and subjected to ICC with the ELAVL1-specific monoclonal antibody and the pan-YPEL antibody. DAPI staining indicates the nucleus. The scale bar is 20 µm. (e) To assess the effect of the reduced levels of ELAVL1 on the size and numbers of SG, cells shown in Figure d were subjected to quantification using the CellProfiler image analysis program. Asterisks indicate significant changes ($p < 0.0001$).

YPEL in SGs, we transiently transfected COS7 with AllStar control siRNA (AS-siR) or a siRNA pool that targets ELAVL1, EL1-siR, for 24 h. WB analysis indicated that EL1-siR effectively reduces both cytoplasmic and nuclear levels of ELAVL1 (Figure 9a) reflected in ICC as well (Figure 9b). To examine the SG formation, COS7 cells transfected with EL1-siR were treated without (Figure 9c) or with 200 µM SA (Figure 9d) for 1 h. We observed that even in the presence of reduced cytoplasmic levels of ELAVL1 in cells transfected with EL1-siR, YPEL localizes to SG-like structures in response SA (Figure 9d) as observed in cells transfected with AS-siR (Figure 9b). This suggests that YPEL localization to SGs is independent of ELAVL1. Furthermore, we observed that G3BP1 and YPEL co-localize to SGs with smaller

sizes and substantially higher numbers (Figure 9e) in cells transfected with EL1-siR compared to those in cells transfected with the control AS-siR, as reported previously (Jain et al., 2016). This observation implies that ELAVL1 is a critical substrate for the maturation of SGs, as shown previously (Ma et al., 1996; Wu & Xu, 2022).

3 | DISCUSSION

We here initially explored the identification of dynamic YPEL2 protein interaction networks as a means to delineate the functional features of YPEL2 in mediating cellular processes using inducible YPEL2 synthesis in COS7 cells under steady-state conditions followed by dynamic

TurboID-MS analyses. Our results indicate that the proximity interaction partners of YPEL2 encompass proteins involved mainly in RNA metabolic processes. Since the proximity interacting partners of YPEL2 also functionally overlap in processes associated with the formation and disassembly of cytoplasmic RNP granules involved in cellular stress responses, as we observe here with SA, an oxidative stress inducer, we suggest that YPEL2 is involved in stress surveillance mechanisms critical for cellular survival.

Although the YPEL proteins are reported to participate in cellular events, including proliferation, mitochondrial function, morphology, motility, differentiation, senescence, and death (Aerts et al., 2006b; Baek et al., 2021; Baker, 2003; Blanco-Sanchez et al., 2020; Dean et al., 2022; Farlie et al., 2001; Garcíá et al., 2019; Hosono et al., 2010; Jun et al., 2007; K. D. Kelley et al., 2010; J. H. Kim et al., 2020; Kong et al., 2018; J. Y. Lee et al., 2017; W. Li et al., 2022; Liang et al., 2010; Mattebo et al., 2021; Oki et al., 2016; Tan et al., 2015; Tuttle et al., 2012; J. Zhang et al., 2016) studies on YPEL2 are limited. Deregulated expression of *YPEL2* is reported in various pathologies, including ccRCC (L. Wang et al., 2022), breast cancer (K. D. Kelley et al., 2010; Mascia et al., 2022; X. Wang & Wang, 2021), chronic idiopathic urticaria, and active hives (Lin et al., 2017). Using publically available pan-cancer databases, for example, it was reported that *YPEL2*, along with *YPEL1* and *YPEL5*, is differentially expressed in ccRCC and that increased expressions of *YPEL1*, *YPEL2*, and *YPEL5* were associated with improved overall as well as disease-specific survival of ccRCC patients (L. Wang et al., 2022). Experimental studies further suggested the involvement of YPEL1, YPEL2, and YPEL5 in maintaining the characteristics of ccRCC tumors (L. Wang et al., 2022). Similarly, recent studies showed an increased expression of *YPEL2* in human atherosclerotic plaques (J.-X. Xu et al., 2023) and that YPEL2 in response to a stress inducer drives premature senescence of an endothelial cell model by blocking the cell cycle through the activation of the p53/p21 pathway (J.-X. Xu et al., 2023). We here observe that inducible synthesis of YPEL2 in COS7 cells, displaying diffuse intracellular staining encompassing both the nucleus and cytoplasm, induces a temporal stalling of cellular proliferation without affecting cell cycle kinetics or cell death.

However, how YPEL2 exerts its effects on cellular processes is unclear. Our dynamic TurboID-MS analyses as an attempt to infer a function for YPEL2 indicate that proximity interactors of YPEL2 at all time points of biotinylation are involved mainly in RNA metabolic processes, including RNA folding, mRNA maturation, stability, export, translation, and degradation as well as cellular response to stress (Figure 5). Association of YPEL2 with various RNA binding proteins at all time points of biotinylation could constitute a basis for time-specific sequential events, reflected as the generation of temporal enrichments of GO-terms that likely result in alterations of cellular proliferation. For example, in addition to RNA metabolic processes observed at 1 and 3 h biotinylation, we also observe the clustering of YPEL2 proximity interactors in the GO-term of "stress granule (SG) assembly" as well as clustering in the GO-term of "mitotic cell cycle" at 3, 6, and 16 h of biotinylation. SGs and PBs are cytoplasmic ribonucleoprotein (RNP) assemblies, which are membrane-less dynamic networks of multivalent protein–protein and protein-RNA condensates that are formed through liquid–liquid phase separation (LLPS) for RNA storage and/or processing (Hofmann et al., 2021; Luo et al., 2018; Riggs et al., 2020; Standart & Weil, 2018; Tauber et al., 2020; Van Treeck & Parker, 2018). Of RNPs, PBs are constitutively present in the cytoplasm. PBs contain mRNAs that encode proteins involved in various regulatory processes as reservoirs for rapid adaptation to gene expressions in response to internal and external clues (Hubstenberger et al., 2017; Standart & Weil, 2018). Cytoplasmic SGs are formed as defense mechanisms to protect cells against adverse effects of specific stresses, including osmotic and oxidative stresses, which also increase the size and/or number of PBs (Hofmann et al., 2021; Luo et al., 2018; Riggs et al., 2020; Standart & Weil, 2018; Tauber et al., 2020; Van Treeck & Parker, 2018). In stressed cells, PBs are often found adjacent to SGs and exchange content with each other and the cytoplasm (Hofmann et al., 2021; Luo et al., 2018; Riggs et al., 2020; Standart & Weil, 2018; Tauber et al., 2020; Van Treeck & Parker, 2018). SG-associated proteome and transcriptome profiles show that SGs sequester primarily untranslated mRNPs derived from mRNAs stalled in translation initiation, including pre-initiation complexes for storage during a period of stress, and once the stress is attenuated for re-initiation of translation or degradation through autophagy (Hofmann et al., 2021; Luo et al., 2018; Riggs et al., 2020; Standart & Weil, 2018; Tauber et al., 2020; Van Treeck & Parker, 2018). It is therefore suggested that SGs are critical for translation reprogramming by dynamically partitioning translationally silenced mRNAs enabling the preferential translation of priority mRNAs from the cytoplasm or stored pool in PBs in response to cellular stress (Hofmann et al., 2021; Riggs et al., 2020; Standart & Weil, 2018). We observed under steady-state conditions in COS7 cells that a substantial portion of proximal interactors of YPEL2 at all time points coincided with proteins critical for the formation/resolution of PB and SG, including ELAVL1 which we verified with interactions and co-localizations of YPEL2 under both steady-state

and oxidative stress conditions. These observations collectively suggest that YPEL2 is involved in cellular stress surveillance.

What might be the underlying mechanism(s) for the involvement of YPEL2 in cellular stress responses? Our in silico analyses indicate that YPEL2, like other YPEL proteins, possesses only a single structural feature: the Yippee domain (Figure 1). Homology modeling, as an attempt to infer a function(s) for YPEL2 through the Yippee domain, also known as MeDIY (Spiller et al., 2017) or CULT/β-tent fold domain (Lupas et al., 2015), indicated matches for proteins with oxidoreductase, RNA binding/hydrolase, and chaperon functions in several protein families of prokaryotes and eukaryotes. The presence of yippee-like globular domains in oxidoreductase MSRA/MSRB proteins of prokaryotes and eukaryotes, E3 ligase cereblon protein, RNA helicases DHR-3, RIG-I/DHX58, and MDA5 proteins, as well as chaperon MSS4/RABIF protein of eukaryotes, likely indicate an evolutionary relationship, as suggested (Lupas et al., 2015; Subramanian et al., 2016). However, distinct ligand specificities evolutionarily conserved the yippee domain of these proteins also render predictions on the physiological ligand(s) for YPEL2 difficult.

Despite the Yippee fold, differences in amino acid compositions of the Yippee fold in proteins could generate specialized molecular interaction networks that drive the formation of discrete interacting surfaces, resulting in selective ligand recognition. One functional feature for YPEL2 predicted by our homology modeling involves oxidoreductase activity derived from the evolutionary conserved MSRA and MSRB proteins of eukaryotes (Burhans & Heintz, 2009; Espinosa-Diez et al., 2015). As YPEL2 localizes within stress granules in response to SA, an oxidative stress inducer, and may involved in stress granule-related processes, it is plausible that YPEL2 may serve as a "reader/sensor" for reactive oxygen species (ROS) generated during oxidative stress. ROS are formed as physiological metabolic by-products of oxidation–reduction reactions mediated by a large number of oxidase enzymes and the mitochondrial electron transport chain (Burhans & Heintz, 2009; Espinosa-Diez et al., 2015; Sies et al., 2022). The effects of ROS in cells manifest mainly in the reversible oxidation of methionine, cysteine, selenoproteins, lipids, and RNA/DNA, leading to modification of substrate activities (Burhans & Heintz, 2009; Espinosa-Diez et al., 2015; Sies et al., 2022). ROS formation and subsequent degradation are regulated by cellular defense systems capable of removing oxidants or their precursors (Burhans & Heintz, 2009; Espinosa-Diez et al., 2015; Sies et al., 2022). Increased levels of ROS that exceed the ability of the cell defense system to remove oxidants result in the activation of intracellular

signaling pathways for removal of, or adaptation to, stress or stress-induced cell death (Espinosa-Diez et al., 2015; Sies et al., 2022). Methionine, for example, in proteins acts as a reversible redox switch, constituting a vital antioxidant defense mechanism that affects many cellular functions. Methionine can be oxidized to methionine sulfoxide either non-specifically by ROS or as a specific, enzyme-catalyzed post-translational modification altering the local conformation of proteins (Espinosa-Diez et al., 2015; Sies et al., 2022). The MSRA and MSRB enzymes reduce methionine sulfoxide to generate unmodified methionine. Despite the Yippee fold, it is unlikely that YPEL2 is a member of the methionine-sulfoxide reductase family as it lacks the invariably conserved cysteine-containing motifs essential for the catalytic activity of MSRA (GCPWG) or the MSRB (RXCXN) proteins (H. Y. Kim & Gladyshev, 2004; B. C. Lee et al., 2009; X. H. Zhang & Weissbach, 2008). Nevertheless, the yippee domain of YPEL2 as a "reader/sensor" could be associated with oxidized methionine in free form or proteins.

The possible "reader/sensor" function of YPEL2 could also be the case for the oxidization of cysteine residues of cellular proteins. As methionine, cysteine is a redox-sensitive site that ROS can covalently modify through reversible and irreversible oxidation (Giles et al., 2003; Paulsen & Carroll, 2013). Due to the unique chemical characteristics of its thiol group, cysteine plays also a crucial role in the structure of proteins and protein-folding pathways through intra- and inter-molecular linkages with other cysteine residues. For example, cysteine oxidation of the SG-nucleating protein TIA1 is shown to lead to oligomerization and subsequent inhibition of SG assembly that promotes apoptosis (Arimoto-Matsuzaki et al., 2016). This finding also lends credence to the conclusion that removing oxidation-induced damage on proteins is critical for cell survival. SQSTM1, one of the YPEL2 interacting partners, is a prototypical autophagic receptor that links ubiquitylated substrates to the nascent autophagic vesicles for cell survival (Kumar et al., 2022). Studies indicate that oxidation of cysteine residues in SQSTM1 in response to hydrogen peroxide, H_2O_2, at low concentrations triggers rapid but transient SQSTM1 oligomerization, in contrast to high concentrations that lead to aggregation and subsequent degradation of SQSTM1 with its ubiquitinated substrates through autophagy (Carroll et al., 2018). Moreover, TARDBP, as one of the YPEL2 proximity interactors, also acts as an RBP. Cysteine oxidation of one of the RNA recognition motifs of TARDBP results in the loss of function by fragmentation and accumulation of fragments in insoluble aggregates (Chang et al., 2013). Furthermore, BAG6 is a member of the Bcl-2 associated athanogene family, an evolutionarily

conserved, multifunctional group of co-chaperone regulators, including BAG2 and BAG3, which are YPEL2 proximal interactors. BAG6 functions in the prevention of the aggregation of misfolded hydrophobic patch-containing proteins as a part of a cytosolic protein quality control complex (Stürner & Behl, 2017). It appears that BAG6 as a sensor for fragments of TARDBP facilitates the ubiquitylation of fragments for degradation, thereby preventing their intracellular aggregation (Kasu et al., 2022).

The possible "reader/sensor" function for YPEL2 of redox homeostasis is supportive of our observation that YPEL2 interacts with the members of the RIG-I/MDA5/ZCCHC3/TRIM25 complex, which counteracts viral infection-generated increases in ROS levels (Schwarz, 1996). Members of the RIG-I-like RNA helicase (RLR) family, including DRH3 of *Caenorhabditis elegans*, the human RIG-I/DHX58, and MDA5 proteins, are involved in the endogenous RNAi biogenesis as well as in recognition of cytoplasmic viral RNA as sensors. This family of proteins possesses a central helicase domain and a carboxyl-terminally located Yippee domain (also referred to as the regulatory domain, RD) with different RNA binding specificities (Rehwinkel & Gack, 2020) due to the protein-specific regional conformation (Lu et al., 2011). DRH3, for example, binds both single-stranded and double-stranded RNAs independently of 5′-triphosphate (Matranga & Pyle, 2010), whereas the Yippee domain of MDA5 preferentially binds long, capped 5′ mono- or di-phosphate containing double- or single-stranded RNAs. On the other hand, the Yippee domain of RIG-I associates with short double-stranded or 5′-triphosphates of uncapped single- or double-stranded RNAs (Hornung et al., 2006; Rehwinkel & Gack, 2020). Interestingly, as one of the YPEL2 proximity interactors, ZCCHC3 acts as a co-receptor for both RIG-I and MDA5 by binding to RNA and interacting with the Yippee domains of RIG-I and MDA5, thereby enhancing RNA binding of these proteins (Lian et al., 2018). Moreover, the recruitment of E3 ligase TRIM25 to the RIG-I/MDA5/ZCCHC3 complex by ZCCHC3 induces the ubiquitylation and activation of RIG-I and MDA5 (Lian et al., 2018).

The "reader/sensor" function of YPEL2 for oxidized substrates could also be critical for repair processes of oxidative stress-mediated damages/modifications to RNA. In addition to proteins, ROS under both steady-state and oxidative stress conditions induce nucleic acid 8-oxo-guanine (o^8G) modification frequently occurring on coding- and non-coding RNAs, including rRNA and tRNA, than DNA (Hahm et al., 2022; Tanaka & Chock, 2021; Veal et al., 2007; Yan & Zaher, 2019). o^8G modification affects every stage of mRNA metabolism, including RNA folding, maturation processing, stability, export, translation, translation fidelity, and decay (Hahm et al., 2022; Nagarajan et al., 2013; Tanaka & Chock, 2021; Veal et al., 2007; Yan & Zaher, 2019). For instance, XRN1, one of the YPEL2 proximity partners, is a member of the 5′→3′-exoribonucleases family that plays critical roles in mRNA processing and turnover, no-go and nonsense-mediated decay, as well as the RNA interference pathways. It is shown that o^8G modifications induce translation stalling (Simms et al., 2014) and decrease the processing efficiency of XRN1 (Phillips et al., 2021). In addition, ribosome rescue upon translation stalling is carried out by a set of proteins, including ABCE1, a proximity interacting partner of YPEL2, which participates in the alleviation of stalling-induced translational stresses (Pisareva et al., 2011).

One possibility for the possible "reader/sensor" function of YPEL2 also includes the sequestration of ROS. The Yippee domain of YPEL2 contains two cysteine pairs that are 52 amino acids apart (CX_2C-X_{52}-CX_2C) that could fold to form a zinc (Zn^{++}) binding pocket (Figure S11), for example, observed with the MSRB proteins (Abhilash Kumar et al., 2002; H. Y. Kim & Gladyshev, 2004). This Zn^{++}-mediated cysteine residue coordination is critical for forming a stable protein structure and conformation that mediates protein function, protein-DNA, protein-RNA, and protein–protein interactions (Maret, 2006; Pace & Weerapana, 2014). The release of Zn^{++} as a result of the oxidation of cysteine thiols of the Yippee fold of YPEL2 could sequester ROS. Subsequent formation of intra/inter-molecular linkages with other cysteine residues within YPEL2 or other proteins could lead to protein aggregations critical for the removal, elimination, and/or repair of oxidized substrates under both steady-state and oxidative-stress-induced conditions to ensure cell survival, as observed with TIA1 (Arimoto-Matsuzaki et al., 2016) and SQSTM1 (Carroll et al., 2018).

In summary, our results suggest that YPEL2 could act as a sensor/reader for ROS and is involved in stress surveillance critical for cellular proliferation through proximity interactions with protein networks primarily encompassing RNA metabolic processes. Our findings provide a point of departure to delve further into the involvement of YPEL2 in cellular events and also testable predictions about the structure/function of YPEL2. Since stress-mediated increases in ROS act as damaging molecules and are also critical inducers of cellular signaling networks, deciphering the potential function and role of YPEL2 in stress surveillance mechanisms could contribute to a better understanding of the physiology and pathophysiology of cellular stress responses.

4 | MATERIALS AND METHODS

In silico analyses. The alignment of amino acid sequences of human YPEL proteins was generated with the Jalview (Waterhouse et al., 2009) program (https://www.jalview.org/) using the ClustalOmega (Sievers & Higgins, 2021) plug-in (https://www.ebi.ac.uk/Tools/msa/clustalo/). For the tertiary structure prediction and superimposition of the tertiary structures of YPEL1-5 proteins, we used the AlphaFold (Jumper et al., 2021; Varadi et al., 2022) server (https://alphafold.ebi.ac.uk/) with the ChimeraX molecular visualization (Baek et al., 2021; Goddard et al., 2018; Miller & Yelton, 2017; Pettersen et al., 2021) program (https://www.cgl.ucsf.edu/chimerax/). For the homology modeling of YPEL proteins, we used the Phyre2 (L. A. Kelley et al., 2015) protein fold recognition server (http://www.sbg.bio.ic.ac.uk/~phyre2/html/page.cgi?id=index). We also used a Venn diagram tool (https://bioinformatics.psb.ugent.be/webtools/Venn/) to visualize the intersections of proximity interaction partners. Tissue-specific gene expression analyses were conducted using the GTEx portal (https://gtexportal.org/home/). Functional features, interactome profiles, and membership analyses of putative interacting proteins of YPEL2 were carried out with the Metascape (Zhou et al., 2019) portal (https://metascape.org/).

4.1 | Biochemicals

Restriction and DNA modifying enzymes were obtained from New England Bio-Labs (Beverly, MA, USA) or ThermoFisher (ThermoFisher, Waltham, MA, USA). Chemicals were obtained from Sigma-Aldrich (Germany), ThermoFisher, or BioTechne-Tocris Corp. (Minnesota, USA). DNA and RNA isolation kits were purchased from ZymoResearch (California, USA). SYBR Green Supermix kit was procured from Bio-Rad Life Sciences Inc. (California, USA). Pageruler Prestained Protein Ladder (ThermoFisher; 26616) or Pageruler Plus Prestained Protein Ladder (ThermoFisher; 26620) was used as the MM marker. Sodium arsenite (SA, $NaAsO_2$, S7400) was acquired from Sigma-Aldrich Inc. (Missouri, USA).

Monoclonal mouse Flag-M2 antibody (F1804) was purchased from Sigma-Aldrich. Rabbit polyclonal HDAC1 (ab19845), rabbit polyclonal β-actin (ab8227), rabbit polyclonal biotin (ab53494) antibodies, and Alexa Fluor 647-conjugated goat anti-rabbit IgG (ab150083) were acquired from Abcam Inc. (Connecticut, USA). Rabbit polyclonal pan-YPEL (sc-99727), mouse monoclonal G3BP1 (sc-365338), mouse monoclonal ELAVL1 (sc-5261), mouse monoclonal Vimentin (sc-6260), mouse

monoclonal γ-tubulin (sc-17787), mouse monoclonal SQSTM1 (sc-48402) antibodies together with a siRNA poll specific for ELAVL1 transcripts (sc-35619) and HRP-conjugated goat anti-mouse IgG (sc-2005) were purchased from Santa Cruz Biotechnology, Inc. (SCBT, Texas, USA). A rabbit polyclonal antibody specific to G3BP1 (13057-2-AP) was obtained from Proteintech Group (Illinois, USA). We purchased Alexa Fluor 488-conjugated goat anti-mouse IgG (BioLegend 405319) from BioLegend Inc. (California, USA) and HRP-conjugated goat anti-rabbit IgG (Advansta R-05072-500) from Advansta Inc. (California, USA). AllStar negative control siRNA (SI03650318) was purchased from Qiagen Inc. (Germany).

4.2 | Cell lines and growth conditions

The estrogen-responsive and ERα-synthesizing MCF7 cells derived from a breast adenocarcinoma and COS7 cells derived from African green monkey kidney fibroblasts were maintained in high glucose (4.5 g/L) Dulbecco's modified eagle medium (DMEM) without phenol red (Biochrom F0475) supplemented with 10% fetal bovine serum (FBS, Biochrom S0115), 1% penicillin-streptomycin, and 0.5% L-glutamine as we described previously (Ayaz et al., 2020; Muyan et al., 2001). To test the effects of ligands on expressions of the YPEL family genes expressions in MCF7 cells, we used E2 (Sigma-Aldrich, E2758) and Imperial Chemical Industries (ICI) 182,780, (BioTechne-Tocris, 1047), a complete antagonist for ERα. For 10^{-9}M E2 and/or 10^{-7}M ICI treatments, MCF7 cells were grown in DMEM supplemented with charcoal-dextran-stripped FBS (CD-FBS) to reduce endogenous steroid hormone content. For the induction of transgene expression by doxycycline (Dox), COS7 cells were maintained and transfected in the DMEM medium containing 10% tetracycline-free FBS (Tet-free FBS, Biowest, France, S181T) to minimize the effect of endogenous tetracycline on transgene expression. Media of cultured cells incubated in a humidified incubator with 5% CO_2 at 37°C were refreshed every 3 days. Cells were passaged for a maximum of eight passages.

4.3 | RNA isolation and RT-qPCR

Total RNA isolation was performed with QuickRNA Miniprep Kit (ZymoResearch) according to the manufacturer's instructions, including on-column DNase I digestion as we described (Yaşar et al., 2016). Isolated total RNA from MCF7 cells treated without (ethanol control) or with 10^{-9}M E2 and/or 10^{-7}M ICI for 24 h was used

for cDNA synthesis (The RevertAid First Strand cDNA Synthesis Kit, Thermo-Fisher) with oligo $(dT)_{18}$ primers according to manufacturer's instructions. We also used total RNA from COS7 cells maintained under the steady-state condition for cDNA synthesis. The expression of YPEL transcripts was then assessed with RT-qPCR using transcript-specific primer sets (Table S1) and the SsoAdvanced Universal SYBR Green Supermix kit (Bio-Rad). Expression levels of transcripts were assessed with the efficiency corrected form of the $2^{-\Delta CT}$ method and normalized using the *RPLP0* expression levels (Livak & Schmittgen, 2001). Relative expression levels of YPEL genes were evaluated using the $2^{-\Delta\Delta CT}$ method (Livak & Schmittgen, 2001) and normalized using the *RPLP0* expression levels. Results were arbitrarily adjusted to the expression level of YPEL1. In all RT-qPCR experiments, MIQE Guidelines were followed (Bustin et al., 2009).

4.4 | Cloning

For the cloning of ORFs of *YPEL1-YPEL5*, we used RefSeq mRNA sequences obtained from the NCBI database, which were aligned with the MUSCLE (MUltiple Sequence Comparison by Log-Expectation) software (Edgar, 2004). Two sets of primers using NCBI Primer Blast (https://www.ncbi.nlm.nih.gov/tools/primer-blast/) were generated for each gene based on the sequences in the NCBI database. The first set of primers consisted of a forward primer from 5′UTR and a reverse primer from 3′UTR. The second set of primers, internal to the first set of primers, nested primers, contained restriction enzyme sites designed to provide flexibility in cloning. For YPEL3, we also used transcript variant 1, which has the identical core sequence of transcript variant 2, containing an extended 5′ sequence that encodes an additional 38 amino acids at the amino terminus. In the engineering of all constructs, the first ATG was designed to be embedded into the consensus Kozak sequence (CCATGG) for efficient translation; reverse cloning primers were also designed to contain a polyA signal (TAATAAA) that comprises a stop codon as we described previously (Ayaz et al., 2021; Yaşar et al., 2016; Yi et al., 2002). The generated YPEL cDNAs were then cloned into the pcDNA 3.1 (−) vector. We also cloned YPEL cDNAs into the pcDNA 3.1(−) vector bearing in-frame sequences encoding for an amino-terminally located 3xFlag (3F) tag at the 5′-end of the MCS. All constructs were sequenced for the fidelity of encoding sequences. All primer sequences are given in Table S1.

For inducible expression of the YPEL2 cDNA, we used a tetracycline-responsive expression system, pINDUCER20 (Meerbrey et al., 2011), obtained from Addgene (Plasmid #44012; Massachusetts, USA). pINDUCER20 is a single vector system that encodes the reverse tetracycline-controlled transactivator (rtTA3) and the neomycin resistance gene as a constitutive, bicistronic transcript (Meerbrey et al., 2011). rtTA3 binds to and activates transgene expression from the TRE promoter, which is a seven-repeat of a 19-nucleotide long tetracycline operator (tetO), only in the presence of tetracycline or the stable tetracycline analog doxycycline, Dox. We modified pINDUCER20 by inserting a DNA fragment bearing a MCS on gateway destination sequences for easy cloning of the gene of interest (pINDUCER20-MCS). We then cloned 3F-YPEL2 cDNA into the pINDUCER20-MCS and sequenced it to ensure the sequence fidelity.

To obtain time-dependent profiling of stable, transient, and/or weak protein interactions of YPEL2, we initially generated a TurboID-HA cDNA using the 3xHA-TurboID-NLS-pcDNA3 (Branon et al., 2018) expression vector (Plasmid #107171; Addgene, Massachusetts, USA) as the template. The TurboID-HA cDNA was generated by PCR with a primer containing sequences encoding a carboxyl-terminally located HA tag with a stop codon present in a polyA motif (TAATAAA) and a primer encoding sequences with or without the initiation methionine codon (iMet). In this engineering, we aimed to generate transgene proteins displaying overlapping intracellular locations, thereby minimizing false-negative results (Figure S4). The TurboID-HA amplicon with the iMet codon was cloned with appropriate restriction enzyme sites into pcDNA3.1(−) to generate pcDNA-TurboID-HA. We then cloned the 3F-YPEL2 cDNA into pcDNA-TurboID-HA to obtain the pcDNA-3F-YPEL2--TurboID-HA expression vector. The constructs were sequenced for sequence fidelity. To dictate the timing and the level of protein synthesis in transiently transfected cells to minimize potential adverse effects of transgene overexpression, we also cloned the 3F-YPEL2, 3F-YPEL2-Turbo-HA, or Turbo-HA cDNA into pINDUCER20-MCS.

Immunocytochemistry (ICC) and western blot (WB). To assess the intracellular location of transgene products, we transiently transfected COS7 cells with the expression vector pcDNA3.1(−) bearing none (EV) or a cDNA for 3F-YPEL2, Turbo-HA or 3F-YPEL2-TurboID-HA. Cells after a 24-hour transient transfection were processed for ICC and WB analyses as we described previously (Ayaz et al., 2020). In brief, for ICC, cells on coverslips were washed three times with $1\times$ PBS and fixed with 3.7% formaldehyde for 30 min. Cells were then permeabilized with 0.4% Triton-X-100 for 10 min. Blocking was performed with 10% Bovine Serum Albumin (BSA) for 1 h. The Flag (1:250, Sigma Aldrich, F-1804) in 3% BSA, the

HA (1:500, Abcam ab9119), or the Biotin (1:500, in 3% BSA, Abcam ab53494) primary antibody in 3% BSA was added sequentially onto the cells for 2 h. Cells were washed three times with 1× PBS and incubated with a secondary antibody for 30 min each. An Alexa Fluor 488-conjugated goat anti-mouse (1:1000 in 3% BSA; Abcam ab150113) for the Flag antibody or an Alexa Fluor 594-conjugated goat anti-rabbit secondary antibody (1:1000 in 3% BSA; Abcam ab150080) for the HA or the Biotin antibody was used. After three 1x PBS washes, coverslips were mounted onto the glass slides with the Fluoroshield Mounting Medium containing 4′,6-diamidino-2-phenylindole (DAPI). Imaging was carried out with a Nikon Eclipse 50i Fluorescence Microscope. For WB analysis, equal amounts (50 μg) of cellular extracts were subjected to Sodium Dodecyl Sulfate (SDS)-10% Polyacrylamide Gel Electrophoresis (PAGE), and proteins were scanned with the Flag antibody for 3F-YPEL2 and 3F-YPEL2-Turbo-HA or the HA antibody for Turbo-HA. To assess the incorporation of biotin into the endogenous proteins, cells transfected with pcDNA-3F-YPEL2-Turbo-HA expression vectors for 24 h were incubated without or with 50 μM biotin in the presence of 1 mM ATP for 3 or 16 h. Equal amounts of cellular extracts were then subjected to WB analysis using a biotin antibody (1:5000 dilution, Abcam ab53494).

4.5 | Assessing the effects of YPEL2 on cellular growth

To assess the effects of YPEL2 on cellular growth, 6×10^4 COS7 cells grown in six-well culture plates for 48 h were transiently transfected with pINDUCER20-MCS vector bearing none (EV), or the 3F-YPEL2 cDNA for 24 h. Cells were then incubated in a fresh medium without or with 10 ng/mL Dox for 96 h, refreshing every 24 h. At the end of the experiment, cells were collected by trypsinization, and a portion of cells was subjected to counting using a hemocytometer as described previously (Ayaz et al., 2020; Nott et al., 2009) or subjected to crystal violet staining (Cold Spring Harbor Protocols, 2016) at 96 h. We also subjected cellular extracts collected every 24 h to WB analysis to ensure that cells synthesize 3F-YPEL2 in response to Dox at similar levels throughout the experiment.

In assessing the effects of YPEL2 on cell cycle distribution, we used flow cytometry as we described previously (Ayaz et al., 2020). In short, transfected cells, as described for cellular growth for 24 h, were collected with trypsinization, washed with PBS, and pelleted. Cells were gently re-suspended in 100 μL of 2%CD-FBS containing PBS, fixed, and permeabilized with ice-cold 70% ethanol overnight. Cells were subsequently incubated with 200 μL of PBS containing propidium iodide (20 μg/mL; Sigma-Aldrich), 200 μg/mL RNase A (Thermo-Fisher), and 0.1% (v/v) Triton X-100 (AppliChem, Germany) for 30 min. Cell cycle analyses were then carried out with flow cytometry (BD Accuri C6 Cytometer; BD Biosciences, San Jose, CA, USA).

We used Tonbo APC Annexin V Apoptosis Detection Kit (Cytek Biosciences, The Netherlands) for the Annexin V staining. Transfected cells, as described for cellular growth for 24 h, were harvested and washed twice with cold 1X PBS and then re-suspended in 1 mL Stain Buffer. Cells were centrifuged at room temperature at 300–400× g for 5 min. The cell pellet was resuspended in 100 μL Annexin V Binding Buffer (1X). PE-APC Annexin V conjugate (5 μL) and 7-Amino-Actinomycin (7-ADD) solution (5 μL) were then added to 100 μL of cell suspension, which was gently mixed and incubated for 15 min at room temperature in the dark followed by the addition of 400 μL of 1X binding buffer. Cells were then subjected to flow cytometry (BD Accuri C6 cytometer, BD Biosciences). We also used apoptosis inducer doxorubicin (DRC) at 10 or 100 μM concentration for 24 h as a control for the induction of apoptosis in un-transfected (UT) cells.

4.6 | Dynamic analyses of the putative YPEL2 proximity protein partners

To identify proximity interaction partners of YPEL2, COS7 cells ($2 \times 10^6/10$ cm^2 culture dish of a total of four culture dishes) grown for 48 h were transiently transfected with pINDUCER20-MCS vector bearing none (EV), the Turbo-HA, or the 3F-YPEL2-Turbo-HA cDNA for 24 h. Cells were then subjected to 10 ng/mL Dox treatment for 24 h. Cells were incubated in a fresh medium containing 50 μM Biotin 1 mM ATP for 1, 3, 6, or 16 h with 10 ng/mL Dox. At the end of a time point, cells were collected with trypsinization and pelleted. Pellets were then washed twice with ice-cold 1× PBS and lysed at RT in 400 μL lysis buffer (50 mM Tris, pH 7.4; 500 mM NaCl; 0.4% SDS; 5 mM EDTA; 2% TritonX; 1 mM DTT with freshly added protease [Roche; 5892970001] and phosphatase [Roche; 4906845001]) inhibitors. Cell lysates were sonicated for a total of 7.5 min (with 10-s pulse and 15-s rest in between pulses) and centrifuged at 7500 rpm for 10 min at 4°C. Protein concentrations were assessed with the QuickStart Bradford Protein assay, and 6 mg of protein samples were incubated with 500 μL Streptavidin magnetic beads (NEB, S1420S) overnight. Beads were collected with a magnetic rack and washed twice with Wash Buffer I (2%

SDS in water) for 10 min. Beads were then washed once with Wash Buffer II (2% deoxycholate; 1% TritonX; 50 mM NaCl; 50 mM HEPES pH 7.5; 1 mM EDTA) for 10 min, once with Wash Buffer III (0.5% NP-40; 0.5% deoxycholate; 1% TritonX; 500 mM NaCl; 1 mM EDTA; 10 mM Tris pH 8.0) for 10 min, and once with Wash Buffer IV (50 mM Tris, pH 7.4; 50 mM NaCl) for 30 min at RT. A fraction, 5%, of bound proteins were eluted from the streptavidin beads with 50 μL of Laemmli-DTT sample buffer containing 500 nM D-Biotin for WB analyses using the biotin antibody (Ab533494), and the remaining samples were subjected to MS analyses. Experiments were carried out two independent times.

Protein identification by mass spectrometry. MS analyses were carried out at the Koç University Proteomic Facility (Istanbul, Türkiye) as we described previously (Ayaz et al., 2021). The protein-bound streptavidin beads were washed with 50 mM NH_4HCO_3, followed by reduction with 100 mM DTT in 50 mM NH_4HCO_3 at 56°C for 45 min, and alkylation with 100 mM iodoacetamide at RT in the dark for 30 min. MS Grade Trypsin Protease (Pierce) was added onto the beads for overnight digestion at 37°C (enzyme: protein ratio of 1:100). The resulting peptides were purified using C18 StageTips (ThermoFisher). Peptides were analyzed by C18 nanoflow reversed-phase HPLC (2D nanoLC; Eksigent) linked to a Q-Exactive Orbitrap mass spectrometer (ThermoFisher). The data sets were searched against the human SWISS-PROT database version 2019_02. Proteome Discoverer (version 1.4; ThermoFisher), employing both the Mascot and Sequest search engines, was used to identify and quantify peptides. Trypsin was specified as the hydrolytic enzyme in the search process, allowing for a maximum of two missed cleavages. For peptide identification, the mass tolerances were set at ±10 ppm for precursor masses and ±0.02 Da for fragment ions. To ensure data reliability, false discovery rates (FDR) for peptide and protein identifications were established at 1%, accomplished through the Percolator node within the Proteome Discoverer. Additionally, a stringent filter was employed to accept only those peptide identifications with medium to high confidence levels, requiring a minimum sequence length of 6, a Mascot score exceeding 20, and a peptide rank of 1. The final protein lists were analyzed using the STRING v11.5 (Szklarczyk et al., 2021) and DAVID v2022q4 (Sherman et al., 2022) databases.

4.7 | Assessing the interaction of putative interaction protein partners with YPEL2

To discern YPEL2-specific proximity interactors, we employed a subtractive analysis approach. This approach involved the inclusion of two critical control groups in our TurboID experiments: (1) untransfected (UT) cells and (2) transfected cells synthesizing TurboID-HA. The UT control accounted for potential artifacts or background signals in MS data, which could arise from endogenous residual biotin, while the Turbo-HA control enabled the identification of proteins biotinylated nonspecifically by the enzyme alone. We compared the protein profiles of each biological replicate at each time point from cells synthesizing 3F-YPEL2-TurboID-HA, group 3, with the protein profiles of the control groups. Subsequent subtraction of all common/intersecting protein identities observed in all three groups as false positives allowed us to define YPEL2-specific proximity interactors. Results suggested that YPEL2 interacts with many proteins with or without overlapping patterns at different time points. Based on their functional properties and being common at different biotinylation time points, we initially selected ADSS (Adenylosuccinate Synthase), EEF1D (Eukaryotic Translation Elongation Factor 1 Delta), G3BP1 (G3BP Stress Granule Assembly Factor 1), ELAVL1 (ELAV-like RNA Binding Protein 1), and SQSTM1 (Sequestosome1) to verify that they are interacting partners of YPEL2.

Secondary neighbor analysis entails the identification of neighboring proteins functionally associated with at least two of the YPEL2 proximity interactors using the STRING (Szklarczyk et al., 2023) database (https://string-db.org/). In identifying secondary neighbor proteins, the curated database and experimental scores of known protein–protein interactions were used as thresholds. Protein–protein interactions with curated databases or experimental scores above 900 were selected for secondary neighbors. For visualization of protein networks, including primary and secondary neighbors, we used the Cytoscape (Shannon et al., 2003) network visualization and analysis tool (http://www.cytoscape.org/). When visualizing the dynamic protein network of YPEL2, the primary neighbors were colored in red, the secondary neighbors were colored in green, and the proteins not seen at that time interval were indicated as gray for each hour (1, 3, 6, and 16 h). The CommunityClustering (Glay) (Su et al., 2010) option of the clusterMaker tool, available as a plug-in in Cytoscape, was used for clustering proteins. By supplementing existing clustering functions and providing structured and informative visualization of large networks, GLay provides layout algorithms optimized for large networks. After clustering the proteins, to observe which biological processes the proteins in these clusters are involved in, the GOTerm Biological Process annotations of each cluster were determined by using the BINGO analysis (Maere et al., 2005) tool available in Cytoscape. To determine the GOTerms,

the hypergeometric test was chosen as the statistical method in the BINGO with the Benjamin and Hochberg False Discovery Rate correction. For the determination of biological process GOTerms, the threshold value was set to 0.05. The heatmap was constructed according to the number of genes enriched in GOTerms using GraphPad Prism.

Cloning. For the generation of cDNAs for ADSS, EEF1D, ELAVL1, G3BP1, and SQSTM1, total RNA from COS7 cells was processed for cDNA, which was used as template in PCR with primer sets designed for each gene based on transcript sequences in the NCBI database (https://www.ncbi.nlm.nih.gov/). PCR amplicons were then cloned into pcDNA 3.1(−) vector that bears in-frame sequences encoding for an amino-terminally located 3F or HA tag at the 5′-end of the MCS with appropriate restriction enzymes. Constructs were then sequenced for sequence fidelity.

Synthesis and intracellular location of putative YPEL2 protein partners. pcDNA 3.1(−) expression vector bearing none (EV) or a cDNA for a putative YPEL2 interaction partner were transiently transfected into COS7 cells and processed for WB or ICC as described above.

Co-immunoprecipitation (Co-IP). Co-IP was carried out as described previously (Ayaz et al., 2021). Briefly, COS7 cells, 6×10^4 cells/well, were seeded into six-well tissue culture plates. Cells were transfected with pcDNA 3.1(−) expression vector (0.5 μg/well) bearing the 3F-YPEL2 cDNA and/or the HA-tagged vector driving the expression of the ADSS, EEF1D, ELAVL1, G3BP1, or SQSTM1 cDNA for 48 h. The total amount of transfected DNA was 1 μg/well in co-transfections. To equalize the total amount of DNA (1 μg/well) in transfections that were carried out with a single construct, 0.5 μg pcDNA 3.1(−) driving a cDNA expression was used together with 0.5 μg pcDNA 3.1(−) bearing no cDNA. Cells were then collected with trypsinization and lysed with M-PER (ThermoFisher; 78,833) containing freshly added protease and phosphatase inhibitors. The protein concentration of lysates was assessed with the Bradford Protein Assay. To block non-specific protein binding to magnetic beads, 500 μg lysates were incubated with non-specific IgG (5 μg) together with 25 μL Protein A/G conjugated magnetic beads at 4°C for 1 h. The supernatant was transferred to a clean 1.5 mL microcentrifuge tube, and the beads were discarded. The pre-cleared lysates were subsequently incubated with 5 μg of the HA or Flag antibody at 4°C overnight and followed by the addition of 25 μL Protein A/G conjugated magnetic beads at 4°C for 1.5 h. The beads were washed twice with 500 μL IP buffer (150 mM NaCl, 10 mM HEPES pH 7.5, 10 mM MgCl$_2$, 0.5% Igepal, and protease and phosphatase inhibitors). Bead pellets were resuspended in 30 μL of 2xLaemmli-SDS buffer (187.5 mM Tris–HCl [pH 6.8], 6% [w/v] SDS, 30% glycerol, 150 mM DTT, 0.03% [w/v] bromophenol blue, 2% β-mercaptoethanol) and incubated at 95°C for 5 min. Samples were then applied to a magnetic field for 30 s, and supernatants were subjected to SDS-10% PAGE for WB analysis using the Flag or the HA antibody followed by the HRP-conjugated VeriBlot (Abcam, ab131366). We also carried out Co-IP with the reverse tag constructs to ensure that the interactions between proteins are not due to specific tags.

Proximity ligation assay. To further verify the interaction between YPEL2 and ELAVL1 or SQSTM1, we carried out a PLA assay using the Duolink In Situ Red Starter kit (Sigma-Aldrich) as described previously (Ayaz et al., 2021). In brief, COS7 cells (2.5×10^4) grown on glass coverslips in a well of a 12-well tissue culture plate for 48 h were transiently transfected with the expression vectors bearing none, the 3F-YPEL2 and/or HA-ELAVL1, and/or HA-SQSTM1 cDNA for 48 h. Cells were then fixed with 3.2% PFA in PBS for 10 min, permeabilized with 0.1% Triton-X for 5 min, and then blocked with Duolink blocking solution at 37°C for 30 min. Cells were subsequently probed with the Flag (1:250) and/or the HA (1:500) antibody overnight at 4°C. Cells were then treated with fluorescent probes for 1 h at 37°C. Cells were washed with wash buffer A for 10 min at RT and incubated with secondary antibodies conjugated to plus and minus PLA probes for 1 h at 37°C. After repeating the washing step with wash buffer A for 10 min at RT, cells were incubated with the ligase for 30 min at 37°C. Cells were then incubated with the polymerase in the amplification buffer for 100 min at 37°C. Cells were washed in 1× wash buffer B for 20 min and then with 0.01× wash buffer B for 1 min at RT. Duolink In Situ Mounting media containing DAPI was used for nuclear staining. Images were captured with a Nikon Eclipse 50i Fluorescence Microscope. ImageJ software was used for image analysis.

4.8 | Assessing the formation of SGs

SGs are dynamic phase-separated, membrane-less cytoplasmic ribonucleoprotein assemblies that promote cell survival by condensing translationally stalled mRNAs, ribosomal components, translation initiation factors, and RBPs (Decker & Parker, 2012; Luo et al., 2018; Protter & Parker, 2016). To assess the formation of SGs in COS7 cells in response to various concentrations (0–400 μM) of sodium arsenite (NaAsO$_2$, SA, Sigma Aldrich, S7400) as an oxidative stress inducer, we initially examined the intracellular localization of G3BP1 as one of the canonical SG nucleating factors (Wheeler et al., 2016)

(Figure S10). For ICC, COS7 cells grown on coverslips in 12-well tissue culture plates were treated without or with 100, 200, and 400 μM SA for 1 h. Cells were fixed, washed, blocked, and incubated with a mouse monoclonal G3BP1 antibody (SCBT, sc-365338) followed by an AlexaFluor 488-conjugated goat anti-mouse secondary antibody (BioLegend, 405319). Images were captured with a fluorescence microscope. Results revealed that 200 μM SA is the optimal concentration for inducing SG-like foci in cells without causing cell death. Based on these preliminary studies, we selected 200 μM of SA as the optimal amount to induce SG formation following 1 h treatment.

To further ensure the identity of SGs, we carried out RNA-fluorescence in situ hybridization (RNA-FISH) with an ATTO488-conjugated oligo-dT (50 nucleotides in length) probe (Integrated DNA Technologies, IDT, Belgium) for mRNA detection followed by the identification of the G3BP1 protein with ICC. Cells were then fixed in 3.7% formaldehyde in PBS at room temperature for 30 min and permeabilized with 0.4% Triton-X in PBS for 10 min. Cells were washed twice with $1\times$ PBS and twice with $2\times$ saline sodium citrate (SSC) for 5 min. Cells were subsequently incubated with the ATTO488 conjugated oligo-$(dT)_{50}$ probe (16 ng/μL) in hybridization buffer (%50 Formamide, 10% w/v Dextran sulfate, 1 mg/mL Salmon sperm diluted in 2xSSC) at 37°C overnight. Cells were washed with 2x SSC (2×5 min) and $1\times$ PBS (2×5 min). Images were captured with a fluorescence microscope.

Assessing co-localization of YPEL and ELAVL1 or G3BP1 in SGs in response to SA. To examine the localization of endogenous YPEL proteins in SGs in response to SA for 1 h, COS7 cells grown on coverslips were subjected to ICC using the pan-YPEL (sc-99727), ELAVL1 (sc-5261), and/or G3BP1 (sc-365338) antibody. We used an Alexa Fluor-647 conjugated secondary antibody for the pan-YPEL antibody and/or a secondary antibody conjugated with Alexa Fluor-488 (Biolegend, 405319) for the ELAVL1 (sc-5261) or G3BP1 antibody. Samples were mounted onto glass slides with a mounting medium containing DAPI for imaging with a fluorescence microscope.

Similarly, we assessed the kinetics of SG formation in response to SA and disassembly following SA withdrawal. For the formation of SGs, COS7 cells grown on coverslips were subjected to 200 μM SA for 0, 15, 30, 60, and 120 min and were processed for ICC using the YPEL (sc-99727) or the G3BP1 (sc-365338) antibody. For the disassembly of SG following 1 h of SA treatment (post-stress, PS), cells were washed and maintained in fresh medium without SA for 0, 1, 2, 3, and 4 h. Cells were then fixed and processed for ICC.

To assess the effects of reduced ELAVL1 levels on the co-localization of the endogenous YPEL proteins in SGs, COS7 cells were transiently transfected with 10 nM of a control siRNA (AllStar) or a siRNA pool that targets ELAVL1 transcripts for 24 h. For WB analysis, cell extracts from COS7 cells grown in six-well tissue culture plates were subjected to SDS-10%PAGE followed by WB using the ELAVL1-specific antibody (sc-5261). Proteins were visualized with an HRP-conjugated secondary antibody (BioLegend 405319). For ICC, cells grown on coverslips and transfected with 10 nM of a control siRNA (Qiagen, AllStar, SI03650318) or a siRNA pool that targets ELAVL1 transcripts (sc-35619) for 24 h were subjected to 200 μM SA for 1 h. Cells were then processed for ICC using the ELAVL1 (sc-5261) or a G3BP1 rabbit polyclonal (13057-2-APG3BP1) antibody. Samples mounted onto glass slides with a mounting medium containing DAPI were subjected to visualization using a fluorescence microscope.

Quantification of SGs. To assess the effects of repressed levels of ELAVL1 on the number and size of SGs in the absence or presence of SA, we carried out SG quantification on ICC images using CellProfiler (Stirling et al., 2021) as an open-source image analysis program (http://www.cellprofiler.org). We initially used the Gaussian Filter method to clean up the images from artifact objects by setting the artifact diameter as 5. For nuclei detection ("PrimaryObjects"), we used the global threshold followed by the Otsu threshold. The nucleus was used to identify cytoplasm ("SecondaryObjects") with the Distance-B method as a parameter of 100 pixels outward from the nucleus. Cytoplasm was then extended a few pixels to keep granules present on the cell surface boundaries through "ExpandOrShrinkObjects" modules. We used enhancement with the "EnhanceOrSuppress-Features" module for small circular granules. Enhanced images were finally used to measure the size and number of granules *per* cell in two independent experiments with 100 cells. We used a two-tailed Student's *t*-test with $p < 0.05$ as the limit for statistical significance.

4.9 | Experimental design and statistical rationale

In examining the expression of the YPEL family genes in MCF7 and COS7 cells and the E2 signaling on *YPEL2*, *YPEL3*, and *YPEL5*, all samples were processed as three biological replicates and three technical repeats. Results were analyzed by a two-tailed unpaired Student's *t*-test and depicted as mean $\pm$ SD with a $p < 0.05$ as the limit of statistical significance. Experiments were conducted as three biological replicates to assess the effects of 3F-

YPEL2 on cellular growth and cell cycle distribution. Results were analyzed by a two-tailed unpaired Student's t-test and depicted as mean $\pm$ SD with a $p < 0.05$ as the limit of statistical significance. All other experiments, including dynamic proximity labeling, WB, ICC, and PLA, were conducted at least two independent times.

AUTHOR CONTRIBUTIONS

ACKNOWLEDGMENTS

ORCID

Gizem Turan https://orcid.org/0000-0002-5670-1135
Çağla Ece Olgun https://orcid.org/0000-0002-5380-1851
Mesut Muyan https://orcid.org/0000-0003-3058-6228

REFERENCES

Abdelmohsen K, Srikantan S, Yang X, Lal A, Kim HH, Kuwano Y, et al. Ubiquitin-mediated proteolysis of HuR by heat shock. EMBO J. 2009;28(9):1271–82. https://doi.org/10.1038/emboj.2009.67

Abhilash Kumar R, Koc A, Cerny RL, Gladyshev VN. Reaction mechanism, evolutionary analysis, and role of zinc in Drosophila methionine-R-sulfoxide reductase. J Biol Chem. 2002; 277(40):37527–35. https://doi.org/10.1074/jbc.M203496200

Aerts S, Lambrechts D, Maity S, Van Loo P, Coessens B, De Smet F, et al. Gene prioritization through genomic data fusion. Nat Biotechnol. 2006a;24(6):719. https://doi.org/10.1038/nbt0606-719d

Aerts S, Lambrechts D, Maity S, Van Loo P, Coessens B, De Smet F, et al. Gene prioritization through genomic data fusion. Nat Biotechnol. 2006b;24:537–44. https://doi.org/10.1038/nbt1203

Arimoto-Matsuzaki K, Saito H, Takekawa M. TIA1 oxidation inhibits stress granule assembly and sensitizes cells to stress-induced apoptosis. Nat Commun. 2016;7:10252. https://doi.org/10.1038/ncomms10252

Ayaz G, Razizadeh N, Yaşar P, Kars G, Kahraman DC, Saatci Ö, et al. CXXC5 as an unmethylated CpG dinucleotide binding protein contributes to estrogen-mediated cellular proliferation. Sci Rep. 2020;10:5971. https://doi.org/10.1038/s41598-020-62912-0

Ayaz G, Turan G, Olgun ÇE, Kars G, Karakaya B, Yavuz K, et al. A prelude to the proximity interaction mapping of CXXC5. Sci Rep. 2021;11(1):17587. https://doi.org/10.1038/s41598-021-97060-6

Baek H-S, Kwon T-U, Shin S, Kwon Y-J, Chun Y-J. Steroid sulfatase deficiency causes cellular senescence and abnormal differentiation by inducing Yippee-like 3 expression in human keratinocytes. Sci Rep. 2021;11(1):20867. https://doi.org/10.1038/s41598-021-00051-w

Baker SJ. Small unstable apoptotic protein, an apoptosis-associated protein, suppresses proliferation of myeloid cells. Cancer Res. 2003; 63(3):705–12. http://www.ncbi.nlm.nih.gov/pubmed/12566317

Blanco-Sanchez B, Clement A, Stednitz SJ, Kyle J, Peirce JL, McFadden M, et al. *Yippee like 3* (*ypel3*) is a novel gene required for myelinating and perineurial glia development. PLoS Genet. 2020;16(6):e1008841. https://doi.org/10.1371/journal.pgen.1008841

Boldt K, Van Reeuwijk J, Lu Q, Koutroumpas K, Nguyen TMT, Texier Y, et al. An organelle-specific protein landscape identifies novel diseases and molecular mechanisms. Nat Commun. 2016;7:11491. https://doi.org/10.1038/ncomms11491

Branon TC, Bosch JA, Sanchez AD, Udeshi ND, Svinkina T, Carr SA, et al. Efficient proximity labeling in living cells and organisms with TurboID. Nat Biotechnol. 2018;36(9):880–7. https://doi.org/10.1038/nbt.4201

Burhans WC, Heintz NH. The cell cycle is a redox cycle: linking phase-specific targets to cell fate. Free Radic Biol Med. 2009;47(9): 1282–93. https://doi.org/10.1016/j.freeradbiomed.2009.05.026

Bustin SA, Benes V, Garson JA, Hellemans J, Huggett J, Kubista M, et al. The MIQE guidelines: minimum information for publication of quantitative real-time PCR experiments. Clin Chem. 2009;55:611–22. https://doi.org/10.1373/clinchem.2008.112797

Carroll B, Otten EG, Di M, Stefanatos R, Menzies FM, Smith GR, et al. Oxidation of SQSTM1/p62 mediates the link between redox state and protein homeostasis. Nat Commun. 2018;9(1): 256. https://doi.org/10.1038/s41467-017-02746-z

Chang CK, Chiang MH, Toh EKW, Chang CF, Huang TH. Molecular mechanism of oxidation-induced TDP-43 RRM1 aggregation and loss of function. FEBS Lett. 2013;587(6):575–82. https://doi.org/10.1016/j.febslet.2013.01.038

Crystal violet staining solution (0.5%). Cold Spring Harb Protoc. 2016;2016(4). https://doi.org/10.1101/pdb.rec088328

Colombrita C, Zennaro E, Fallini C, Weber M, Sommacal A, Buratti E, et al. TDP-43 is recruited to stress granules in conditions of oxidative insult. J Neurochem. 2009;111(4):1051–61. https://doi.org/10.1111/j.1471-4159.2009.06383.x

de Bruijn SE, Fiorentino A, Ottaviani D, Fanucchi S, Melo US, Corral-Serrano JC, et al. Structural variants create new topological-associated domains and ectopic retinal enhancer-gene contact in dominant retinitis pigmentosa. Am J Hum Genet. 2020;107(5):802–14. https://doi.org/10.1016/j.ajhg.2020.09.002

Dean DM, Deitcher DL, Paster CO, Xu M, Loehlin DW. "A fly appeared": sable, a classic Drosophila mutation, maps to Yippee, a gene affecting body color, wings, and bristles. G3 (Bethesda). 2022;12(5):jkac058. https://doi.org/10.1093/g3journal/jkac058

Decker CJ, Parker R. P-bodies and stress granules: possible roles in the control of translation and mRNA degradation. Cold Spring Harb Perspect Biol. 2012;4(9):1–16. https://doi.org/10.1101/cshperspect.a012286

Dewulf JP, Marie S, Nassogne MC. Disorders of purine biosynthesis metabolism. Mol Genet Metab. 2022;136(3):190–8. https://doi.org/10.1016/j.ymgme.2021.12.016

Doller A, Pfeilschifter J, Eberhardt W. Signalling pathways regulating nucleo-cytoplasmic shuttling of the mRNA-binding protein HuR. Cell Signal. 2008;20(12):2165–73. https://doi.org/10.1016/j.cellsig.2008.05.007

Edgar RC. MUSCLE: multiple sequence alignment with high accuracy and high throughput. Nucleic Acids Res. 2004;32(5):1792–7. https://doi.org/10.1093/nar/gkh340

Espinosa-Diez C, Miguel V, Mennerich D, Kietzmann T, Sánchez-Pérez P, Cadenas S, et al. Antioxidant responses and cellular adjustments to oxidative stress. Redox Biol. 2015;6:183–97. https://doi.org/10.1016/j.redox.2015.07.008

Farlie P, Reid C, Wilcox S, Peeters J, Reed G, Newgreen D. Ypel1: a novel nuclear protein that induces an epithelial-like morphology in fibroblasts. Genes Cells. 2001;6(7):619–29. https://doi.org/10.1046/j.1365-2443.2001.00445.x

Garcıá SR, Deprez M, Lebrigand K, Cavard A, Paquet A, Arguel MJ, et al. Novel dynamics of human mucociliary differentiation revealed by single-cell RNA sequencing of nasal epithelial cultures. Development (Cambridge). 2019;146(20): dev177428. https://doi.org/10.1242/dev.177428

Giles NM, Watts AB, Giles GI, Fry FH, Littlechild JA, Jacob C. Metal and redox modulation of cysteine protein function. Chem Biol. 2003;10(8):677–93. https://doi.org/10.1016/S1074-5521(03)00174-1

Goddard TD, Huang CC, Meng EC, Pettersen EF, Couch GS, Morris JH, et al. UCSF ChimeraX: meeting modern challenges in visualization and analysis. Protein Sci. 2018;27(1):14–25. https://doi.org/10.1002/pro.3235

Greene LH. Protein structure networks. Brief Funct Genomics. 2012;11(6):469–78. https://doi.org/10.1093/bfgp/els039

Hahm JY, Park J, Jang ES, Chi SW. 8-Oxoguanine: from oxidative damage to epigenetic and epitranscriptional modification. Exp Mol Med. 2022;54(10):1626–42. https://doi.org/10.1038/s12276-022-00822-z

Heminger K, Markey M, Mpagi M, Berberich SJ. Alterations in gene expression and sensitivity to genotoxic stress following HdmX or Hdm2 knockdown in human tumor cells harboring wild-type p53. Aging. 2009;1(1):89–108. https://doi.org/10.18632/aging.100008

Hofmann S, Kedersha N, Anderson P, Ivanov P. Molecular mechanisms of stress granule assembly and disassembly. Biochim Biophys Acta Mol Cell Res. 2021;1868(1):118876. https://doi.org/10.1016/j.bbamcr.2020.118876

Hornung V, Ellegast J, Kim S, Brzózka K, Jung A, Kato H, et al. 5′-Triphosphate RNA is the ligand for RIG-I. Science. 2006; 314(5801):994–7. https://doi.org/10.1126/science.1132505

Hosono K, Noda S, Shimizu A, Nakanishi N, Ohtsubo M, Shimizu N, et al. YPEL5 protein of the YPEL gene family is involved in the cell cycle progression by interacting with two distinct proteins RanBPM and RanBP10. Genomics. 2010;96: 102–11. https://doi.org/10.1016/j.ygeno.2010.05.003

Hosono K, Sasaki T, Minoshima S, Shimizu N. Identification and characterization of a novel gene family YPEL in a wide spectrum of eukaryotic species. Gene. 2004;340(1):31–43. https://doi.org/10.1016/j.gene.2004.06.014

Hubstenberger A, Courel M, Bénard M, Souquere S, Ernoult-Lange M, Chouaib R, et al. P-body purification reveals the condensation of repressed mRNA regulons. Mol Cell. 2017;68(1): 144–157.e5. https://doi.org/10.1016/j.molcel.2017.09.003

Huttlin EL, Bruckner RJ, Paulo JA, Cannon JR, Ting L, Baltier K, et al. Architecture of the human interactome defines protein communities and disease networks. Nature. 2017;545(7655): 505–9. https://doi.org/10.1038/nature22366

Jain S, Wheeler JR, Walters RW, Agrawal A, Barsic A, Parker R. ATPase-modulated stress granules contain a diverse proteome and substructure. Cell. 2016;164(3):487–98. https://doi.org/10.1016/j.cell.2015.12.038

Jumper J, Evans R, Pritzel A, Green T, Figurnov M, Ronneberger O, et al. Highly accurate protein structure prediction with AlphaFold. Nature. 2021;596(7873):583–9. https://doi.org/10.1038/s41586-021-03819-2

Jun D-Y, Park H-W, Kim Y-H. Expression of yippee-like 5 (YPEL5) gene during activation of human peripheral T lymphocytes by immobilized anti-CD3. J Life Sci. 2007;17:1641–8. https://doi.org/10.5352/jls.2007.17.12.1641

Kageyama S, Gudmundsson SR, Sou YS, Ichimura Y, Tamura N, Kazuno S, et al. p62/SQSTM1-droplet serves as a platform for autophagosome formation and anti-oxidative stress response. Nat Commun. 2021;12(1):16. https://doi.org/10.1038/s41467-020-20185-1

Kasu YAT, Arva A, Johnson J, Sajan C, Manzano J, Hennes A, et al. BAG6 prevents the aggregation of neurodegeneration-associated fragments of TDP43. iScience. 2022;25(5):104273. https://doi.org/10.1016/j.isci.2022.104273

Kedersha N, Panas MD, Achorn CA, Lyons S, Tisdale S, Hickman T, et al. G3BP-Caprin1-USP10 complexes mediate stress granule condensation and associate with 40S subunits. J Cell Biol. 2016;212(7):845–60. https://doi.org/10.1083/jcb.201508028

Kelley KD, Miller KR, Todd A, Kelley AR, Tuttle R, Berberich SJ. YPEL3, a p53-regulated gene that induces cellular senescence. Cancer Res. 2010;70(9):3566–75. https://doi.org/10.1158/0008-5472.CAN-09-3219

Kelley LA, Mezulis S, Yates CM, Wass MN, Sternberg MJE. The Phyre2 web portal for protein modeling, prediction and

analysis. Nat Protoc. 2015;10(6):845–58. https://doi.org/10.1038/nprot.2015.053

Kim HY, Gladyshev VN. Methionine sulfoxide reduction in mammals: characterization of methionine-R-sulfoxide reductases. Mol Biol Cell. 2004;15(3):1055–64. https://doi.org/10.1091/mbc.E03-08-0629

Kim JH, Singh M, Pan G, Lopez A, Zito N, Bosse B, et al. Frameshift mutations of YPEL3 alter the sensory circuit function in Drosophila. Dis Model Mech. 2020;13(6):dmm042390. https://doi.org/10.1242/dmm.042390

Kong X, Li Y, Zhang X. Increased expression of the YPEL3 gene in human colonic adenocarcinoma tissue and the effects on proliferation, migration, and invasion of colonic adenocarcinoma cells in vitro via the wnt/β-catenin signaling pathway. Med Sci Monit. 2018;24:4767–75. https://doi.org/10.12659/MSM.908173

Kumar AV, Mills J, Lapierre LR. Selective autophagy receptor p62/-SQSTM1, a pivotal player in stress and aging. Front Cell Dev Biol. 2022;10:793328. https://doi.org/10.3389/fcell.2022.793328

Lamark T, Svenning S, Johansen T. Regulation of selective autophagy: the p62/SQSTM1 paradigm. Essays Biochem. 2017;61(6):609–24. https://doi.org/10.1042/EBC20170035

Lee BC, Dikiy A, Kim HY, Gladyshev VN. Functions and evolution of selenoprotein methionine sulfoxide reductases. Biochim Biophys Acta – Gen Subj. 2009;1790(11):1471–7. https://doi.org/10.1016/j.bbagen.2009.04.014

Lee JY, Jun DY, Park JE, Kwon GH, Kim JS, Kim YH. Pro-apoptotic role of the human YPEL5 gene identified by functional complementation of a yeast moh1Δ mutation. J Microbiol Biotechnol. 2017;27(3):633–43. https://doi.org/10.4014/jmb.1610.10045

Li S, Sun MY, Su X. MIR-885-5p promotes gastric cancer proliferation and invasion through regulating YPEL1. Eur Rev Med Pharmacol Sci. 2019;23(18):7913–9. https://doi.org/10.26355/eurrev_201909_19005

Li W, Huang W, Wu K, Long Y. Yippee like 1 suppresses glioma progression and serves as a novel prognostic factor. Tohoku J Exp Med. 2022;256(2):141–50. https://doi.org/10.1620/tjem.256.141

Li Y, Wang Z, Wu X, Wang G, Gu G, Ren H, et al. Intestinal mucosa-derived DNA methylation signatures in the penetrating intestinal mucosal lesions of Crohn's disease. Sci Rep. 2021;11(1):9771. https://doi.org/10.1038/s41598-021-89087-6

Lian H, Zang R, Wei J, Ye W, Hu MM, Da CY, et al. The zinc-finger protein ZCCHC3 binds RNA and facilitates viral RNA sensing and activation of the RIG-I-like receptors. Immunity. 2018;49(3):438–448.e5. https://doi.org/10.1016/j.immuni.2018.08.014

Liang P, Wan Y, Yan Y, Wang Y, Luo N, Deng Y, et al. MVP interacts with YPEL4 and inhibits YPEL4-mediated activities of the ERK signal pathway. Biochem Cell Biol. 2010;88(3):445–50. https://doi.org/10.1139/O09-166

Lin C-KE, Kaptein JS, Sheikh J. Differential expression of microRNAs and their possible roles in patients with chronic idiopathic urticaria and active hives. Allergy Rhinol. 2017;8(2):67–80. https://doi.org/10.2500/ar.2017.8.0199

Liu-Yesucevitz L, Bilgutay A, Zhang YJ, Vanderwyde T, Citro A, Mehta T, et al. Tar DNA binding protein-43 (TDP-43) associates with stress granules: analysis of cultured cells and pathological brain tissue. PLoS One. 2010;5(10):e13250. https://doi.org/10.1371/journal.pone.0013250

Livak KJ, Schmittgen TD. Analysis of relative gene expression data using real-time quantitative PCR and the $2^{-\Delta\Delta C_T}$ method. Methods. 2001;25:402–8. https://doi.org/10.1006/meth.2001.1262

Lu C, Ranjith-Kumar CT, Hao L, Kao CC, Li P. Crystal structure of RIG-I C-terminal domain bound to blunt-ended double-strand RNA without 5′ triphosphate. Nucleic Acids Res. 2011;39(4):1565–75. https://doi.org/10.1093/nar/gkq974

Luck K, Kim D-K, Lambourne L, Spirohn K, Begg BE, Bian W, et al. A reference map of the human binary protein interactome. Nature. 2020;580(7803):402–8. https://doi.org/10.1038/s41586-020-2188-x

Luo Y, Na Z, Slavoff SA. P-bodies: composition, properties, and functions. Biochemistry. 2018;57(17):2424–31. https://doi.org/10.1021/acs.biochem.7b01162

Lupas AN, Zhu H, Korycinski M. The thalidomide-binding domain of cereblon defines the CULT domain family and is a new member of the β-tent fold. PLoS Comput Biol. 2015;11(1):e1004023. https://doi.org/10.1371/journal.pcbi.1004023

Ma WJ, Cheng S, Campbell C, Wright A, Furneaux H. Cloning and characterization of HuR, a ubiquitously expressed Elav-like protein. J Biol Chem. 1996;271(14):8144–51. https://doi.org/10.1074/jbc.271.14.8144

Maere S, Heymans K, Kuiper M. BiNGO: a Cytoscape plugin to assess overrepresentation of gene ontology categories in biological networks. Bioinformatics. 2005;21(16):3448–9. https://doi.org/10.1093/bioinformatics/bti551

Maret W. Zinc coordination environments in proteins as redox sensors and signal transducers. Antioxid Redox Signal. 2006;8(9–10):1419–41. https://doi.org/10.1089/ars.2006.8.1419

Mascia F, Mazo I, Alterovitz WL, Karagiannis K, Wu WW, Shen RF, et al. In search of autophagy biomarkers in breast cancer: receptor status and drug agnostic transcriptional changes during autophagy flux in cell lines. PLoS One. 2022;17(1):e0262134. https://doi.org/10.1371/journal.pone.0262134

Matranga C, Pyle AM. Double-stranded RNA-dependent ATPase DRH-3: insight into its role in RNA silencing in Caenorhabditis elegans. J Biol Chem. 2010;285(33):25363–71. https://doi.org/10.1074/jbc.M110.117010

Matsuki H, Takahashi M, Higuchi M, Makokha GN, Oie M, Fujii M. Both G3BP1 and G3BP2 contribute to stress granule formation. Genes Cells. 2013;18(2):135–46. https://doi.org/10.1111/gtc.12023

Mattebo A, Sen T, Jassinskaja M, Pimková K, Prieto González-Albo I, Alattar AG, et al. Yippee like 4 (Ypel4) is essential for normal mouse red blood cell membrane integrity. Sci Rep. 2021;11(1):15898. https://doi.org/10.1038/s41598-021-95291-1

Meerbrey KL, Hu G, Kessler JD, Roarty K, Li MZ, Fang JE, et al. The pINDUCER lentiviral toolkit for inducible RNA interference in vitro and in vivo. Proc Natl Acad Sci USA. 2011;108(9):3665–70. https://doi.org/10.1073/pnas.1019736108

Millar SR, Huang JQ, Schreiber KJ, Tsai YC, Won J, Zhang J, et al. A new phase of networking: the molecular composition and regulatory dynamics of mammalian stress granules. Chem Rev. 2022;123:9036–64. https://doi.org/10.1021/acs.chemrev.2c00608

Miller KL, Yelton L. Deep insight into YPEL3. Atlas Genet Cytogenet Oncol Haematol. 2017;(7). https://doi.org/10.4267/2042/62194

Muyan M, Yi P, Sathya G, Willmert LJ, Driscoll MD, Hilf R, et al. Fusion estrogen receptor proteins: toward the development of receptor-based agonists and antagonists. Mol Cell Endocrinol. 2001;182(2):249–63. https://doi.org/10.1016/S0303-7207(01)00493-2

Nagarajan VK, Jones CI, Newbury SF, Green PJ. XRN 5′→3′ exoribonucleases: structure, mechanisms and functions. Biochim Biophys Acta–Gene Regul Mech. 2013;1829(6–7):590–603. https://doi.org/10.1016/j.bbagrm.2013.03.005

Nott SL, Huang Y, Li X, Fluharty BR, Qiu X, Welshons WV, et al. Genomic responses from the estrogen-responsive element-dependent signaling pathway mediated by estrogen receptor α are required to elicit cellular alterations. J Biol Chem. 2009; 284(22):15277–88. https://doi.org/10.1074/jbc.M900365200

Oki K, Plonczynski MW, Gomez-Sanchez EP, Gomez-Sanchez CE. YPEL4 modulates HAC15 adrenal cell proliferation and is associated with tumor diameter. Mol Cell Endocrinol. 2016;434:93–8. https://doi.org/10.1016/j.mce.2016.06.022

Pace NJ, Weerapana E. Zinc-binding cysteines: diverse functions and structural motifs. Biomolecules. 2014;4(2):419–34. https://doi.org/10.3390/biom4020419

Paulsen CE, Carroll KS. Cysteine-mediated redox signaling: chemistry, biology, and tools for discovery. Chem Rev. 2013;113(7): 4633–79. https://doi.org/10.1021/cr300163e

Pettersen EF, Goddard TD, Huang CC, Meng EC, Couch GS, Croll TI, et al. UCSF ChimeraX: structure visualization for researchers, educators, and developers. Protein Sci. 2021;30(1): 70–82. https://doi.org/10.1002/pro.3943

Phillips CN, Schowe S, Langeberg CJ, Siddique N, Chapman EG, Resendiz MJE. Processing of RNA containing 8-oxo-7,-8-dihydroguanosine (8-oxoG) by the exoribonuclease Xrn-1. Front Mol Biosci. 2021;8:780315. https://doi.org/10.3389/fmolb.2021.780315

Pisareva VP, Skabkin MA, Hellen CUT, Pestova TV, Pisarev AV. Dissociation by Pelota, Hbs1 and ABCE1 of mammalian vacant 80S ribosomes and stalled elongation complexes. EMBO J. 2011;30(9):1804–17. https://doi.org/10.1038/emboj.2011.93

Protter DSW, Parker R. Principles and properties of stress granules. Trends Cell Biol. 2016;26(9):668–79. https://doi.org/10.1016/j.tcb.2016.05.004

Rehwinkel J, Gack MU. RIG-I-like receptors: their regulation and roles in RNA sensing. Nat Rev Immunol. 2020;20(9):537–51. https://doi.org/10.1038/s41577-020-0288-3

Riggs CL, Kedersha N, Ivanov P, Anderson P. Mammalian stress granules and P bodies at a glance. J Cell Sci. 2020;133(16): jcs242487. https://doi.org/10.1242/jcs.242487

Roux KJ, Kim DI, Burke B, May DG. BioID: a screen for protein-protein interactions. Curr Protoc Protein Sci. 2018;91(1): 19.23.1–19.23.15. https://doi.org/10.1002/cpps.51

Roux KJ, Kim DI, Raida M, Burke B. A promiscuous biotin ligase fusion protein identifies proximal and interacting proteins in mammalian cells. J Cell Biol. 2012;196(6):801–10. https://doi.org/10.1083/jcb.201112098

Roxström-Lindquist K, Faye I. The Drosophila gene Yippee reveals a novel family of putative zinc-binding proteins highly conserved among eukaryotes. Insect Mol Biol. 2001;10(1):77–86. https://doi.org/10.1046/j.1365-2583.2001.00239.x

Schwarz KB. Oxidative stress during viral infection: a review. Free Radic Biol Med. 1996;21(5):641–9. https://doi.org/10.1016/0891-5849(96)00131-1

Shannon P, Markiel A, Ozier O, Baliga NS, Wang JT, Ramage D, et al. Cytoscape: a software environment for integrated models of biomolecular interaction networks. Genome Res. 2003; 13(11):2498–504. https://doi.org/10.1101/gr.1239303

Sherman BT, Hao M, Qiu J, Jiao X, Baseler MW, Lane HC, et al. DAVID: a web server for functional enrichment analysis and functional annotation of gene lists (2021 update). Nucleic Acids Res. 2022;50(W1):W216–21. https://doi.org/10.1093/nar/gkac194

Sies H, Belousov VV, Chandel NS, Davies MJ, Jones DP, Mann GE, et al. Defining roles of specific reactive oxygen species (ROS) in cell biology and physiology. Nat Rev Mol Cell Biol. 2022;23(7): 499–515. https://doi.org/10.1038/s41580-022-00456-z

Sievers F, Higgins DG. The Clustal Omega Multiple Alignment Package. Methods Mol Biol. 2021;2231:3–16. https://doi.org/10.1007/978-1-0716-1036-7_1

Simms CL, Hudson BH, Mosior JW, Rangwala AS, Zaher HS. An active role for the ribosome in determining the fate of oxidized mRNA. Cell Rep. 2014;9(4):1256–64. https://doi.org/10.1016/j.celrep.2014.10.042

Söderberg O, Leuchowius K-J, Gullberg M, Jarvius M, Weibrecht I, Larsson L-G, et al. Characterizing proteins and their interactions in cells and tissues using the in situ proximity ligation assay. Methods. 2008;45(3):227–32. https://doi.org/10.1016/j.ymeth.2008.06.014

Spiller F, Medina-Pritchard B, Abad MA, Wear MA, Molina O, Earnshaw WC, et al. Molecular basis for Cdk1-regulated timing of Mis18 complex assembly and CENP-A deposition. EMBO Rep. 2017;18(6):894–905. https://doi.org/10.15252/embr.201643564

Spirin V, Mirny LA. Protein complexes and functional modules in molecular networks. Proc Natl Acad Sci USA. 2003;100(21): 12123–8. https://doi.org/10.1073/pnas.2032324100

Standart N, Weil D. P-bodies: cytosolic droplets for coordinated mRNA storage. Trends Genet. 2018;34(8):612–26. https://doi.org/10.1016/j.tig.2018.05.005

Stirling DR, Swain-Bowden MJ, Lucas AM, Carpenter AE, Cimini BA, Goodman A. CellProfiler 4: improvements in speed, utility and usability. BMC Bioinformatics. 2021;22(1):433. https://doi.org/10.1186/s12859-021-04344-9

Stürner E, Behl C. The role of the multifunctional BAG3 protein in cellular protein quality control and in disease. Front Mol Neurosci. 2017;10:177. https://doi.org/10.3389/fnmol.2017.00177

Su G, Kuchinsky A, Morris JH, States DJ, Meng F. GLay: community structure analysis of biological networks. Bioinformatics. 2010; 26(24):3135–7. https://doi.org/10.1093/bioinformatics/btq596

Subramanian L, Medina-Pritchard B, Barton R, Spiller F, Kulasegaran-Shylini R, Radaviciute G, et al. Centromere localization and function of Mis18 requires Yippee-like domain-mediated oligomerization. EMBO Rep. 2016;17(4):496–507. https://doi.org/10.15252/embr.201541520

Sullivan KE. DiGeorge syndrome/chromosome 22q11.2 deletion syndrome. Curr Allergy Asthma Rep. 2001;1(5):438–44. https://doi.org/10.1007/s11882-001-0029-z

Szklarczyk D, Gable AL, Nastou KC, Lyon D, Kirsch R, Pyysalo S, et al. Correction to 'The STRING database in 2021:

customizable protein–protein networks, and functional characterization of user-uploaded gene/measurement sets.' Nucleic Acids Res. 2021;49(18):10800. https://doi.org/10.1093/nar/gkab835

Szklarczyk D, Kirsch R, Koutrouli M, Nastou K, Mehryary F, Hachilif R, et al. The STRING database in 2023: protein–protein association networks and functional enrichment analyses for any sequenced genome of interest. Nucleic Acids Res. 2023;51(D1):D638–46. https://doi.org/10.1093/nar/gkac1000

Tan TY, Gordon CT, Miller KA, Amor DJ, Farlie PG. YPEL1 overexpression in early avian craniofacial mesenchyme causes mandibular dysmorphogenesis by up-regulating apoptosis. Dev Dyn. 2015;244(8):1022–30. https://doi.org/10.1002/dvdy.24299

Tanaka M, Chock PB. Oxidative modifications of RNA and its potential roles in biosystem. Front Mol Biosci. 2021;8:685331. https://doi.org/10.3389/fmolb.2021.685331

Tauber D, Tauber G, Parker R. Mechanisms and regulation of RNA condensation in RNP granule formation. Trends Biochem Sci. 2020;45(9):764–78. https://doi.org/10.1016/j.tibs.2020.05.002

Tourrière H, Gallouzi I, Chebli K, Capony JP, Mouaikel J, van der Geer P, et al. RasGAP-associated endoribonuclease G3BP: selective RNA degradation and phosphorylation-dependent localization. Mol Cell Biol. 2001;21(22):7747–60. https://doi.org/10.1128/mcb.21.22.7747-7760.2001

Tuttle R, Miller KR, Maiorano JN, Termuhlen PM, Gao Y, Berberich SJ. Novel senescence associated gene, *YPEL3*, is repressed by estrogen in ER+ mammary tumor cells and required for tamoxifen-induced cellular senescence. Int J Cancer. 2012;130(10):2291–9. https://doi.org/10.1002/ijc.26239

Tuttle R, Simon M, Hitch DC, Maiorano JN, Hellan M, Ouellette J, et al. Senescence-associated gene YPEL3 is downregulated in human colon tumors. Ann Surg Oncol. 2011;18(6):1791–6. https://doi.org/10.1245/s10434-011-1558-x

Van Treeck B, Parker R. Emerging roles for intermolecular RNA-RNA interactions in RNP assemblies. Cell. 2018;174(4):791–802. https://doi.org/10.1016/j.cell.2018.07.023

Varadi M, Anyango S, Deshpande M, Nair S, Natassia C, Yordanova G, et al. AlphaFold Protein Structure Database: massively expanding the structural coverage of protein-sequence space with high-accuracy models. Nucleic Acids Res. 2022;50(D1):D439–44. https://doi.org/10.1093/nar/gkab1061

Varjosalo M, Keskitalo S, VanDrogen A, Nurkkala H, Vichalkovski A, Aebersold R, et al. The protein interaction landscape of the human CMGC kinase group. Cell Rep. 2013;3(4):1306–20. https://doi.org/10.1016/j.celrep.2013.03.027

Veal EA, Day AM, Morgan BA. Hydrogen peroxide sensing and signaling. Mol Cell. 2007;26(1):1–14. https://doi.org/10.1016/j.molcel.2007.03.016

Vysotskiy M, Zhong X, Miller-Fleming TW, Zhou D, Autism Working Group of the Psychiatric Genomics Consortium^; Bipolar Disorder Working Group of the Psychiatric Genomics Consortium^; Schizophrenia Working Group of the Psychiatric Genomics Consortium^, Cox NJ, et al. Integration of genetic, transcriptomic, and clinical data provides insight into 16p11.2 and 22q11.2 CNV genes. Genome Med. 2021;13(1):172. https://doi.org/10.1186/s13073-021-00972-1

Wakeling AE, Bowler J. Steroidal pure antioestrogens. J Endocrinol. 1987;112(3):R7–R10. https://doi.org/10.1677/joe.0.112R007

Wang L, Zhang Z, Zhou X, Wu J, Hong Z. Comprehensive analysis of the expression and prognosis of YPEL family members in clear cell renal cell cancer. Oncol Rep. 2022;48(1):134. https://doi.org/10.3892/or.2022.8345

Wang X, Wang S. Identification of key genes involved in tamoxifen-resistant breast cancer using bioinformatics analysis. Transl Cancer Res. 2021;10(12):5246–57. https://doi.org/10.21037/tcr-21-1276

Waterhouse AM, Procter JB, Martin DMA, Clamp M, Barton GJ. Jalview Version 2-A multiple sequence alignment editor and analysis workbench. Bioinformatics. 2009;25(9):1189–91. https://doi.org/10.1093/bioinformatics/btp033

Wheeler JR, Matheny T, Jain S, Abrisch R, Parker R. Distinct stages in stress granule assembly and disassembly. eLife. 2016;5:e18413. https://doi.org/10.7554/eLife.18413

Wu X. Up-regulation of YPEL1 and YPEL5 and down-regulation of ITGA2 in erlotinib-treated EGFR-mutant non-small cell lung cancer: a bioinformatic analysis. Gene. 2018;74:643–82. https://doi.org/10.1016/j.gene.2017.12.003

Wu X, Xu L. The RNA-binding protein HuR in human cancer: a friend or foe? Adv Drug Deliv Rev. 2022;184:114179. https://doi.org/10.1016/j.addr.2022.114179

Xu H, Yu S, Peng K, Gao L, Chen S, Shen Z, et al. The role of EEF1D in disease pathogenesis: a narrative review. Ann Transl Med. 2021;9(20):1600. https://doi.org/10.21037/atm-21-5025

Xu J-X, Tang M-L, Lu Z-F, Song Y, Zhang K-L, He R-C, et al. A novel role for YPEL2 in mediating endothelial cellular senescence via the p53/p21 pathway. Mech Ageing Dev. 2023;211:111803. https://doi.org/10.1016/j.mad.2023.111803

Yan LL, Zaher HS. How do cells cope with RNA damage and its consequences? J Biol Chem. 2019;294(41):15158–71. https://doi.org/10.1074/jbc.REV119.006513

Yaşar P, Ayaz G, Muyan M. Estradiol-estrogen receptor α mediates the expression of the *CXXC5* gene through the estrogen response element-dependent signaling pathway. Sci Rep. 2016;6(1):37808. https://doi.org/10.1038/srep37808

Yi P, Bhagat S, Hilf R, Bambara RA, Muyan M. Differences in the abilities of estrogen receptors to integrate activation functions are critical for subtype-specific transcriptional responses. Mol Endocrinol. 2002;16(8):1810–27. https://doi.org/10.1210/me.2001-0323

Youn JY, Dunham WH, Hong SJ, Knight JDR, Bashkurov M, Chen GI, et al. High-density proximity mapping reveals the subcellular organization of mRNA-associated granules and bodies. Mol Cell. 2018;69(3):517–532.e11. https://doi.org/10.1016/j.molcel.2017.12.020

Zhang J, Wen X, Ren XY, Li YQ, Tang XR, Wang YQ, et al. YPEL3 suppresses epithelial-mesenchymal transition and metastasis of nasopharyngeal carcinoma cells through the Wnt/β-catenin signaling pathway. J Exp Clin Cancer Res. 2016;35(1):109. https://doi.org/10.1186/s13046-016-0384-1

Zhang XH, Weissbach H. Origin and evolution of the protein-repairing enzymes methionine sulphoxide reductases. Biol Rev. 2008;83(3):249–57. https://doi.org/10.1111/j.1469-185X.2008.00042.x

Zhou Y, Zhou B, Pache L, Chang M, Khodabakhshi AH, Tanaseichuk O, et al. Metascape provides a biologist-oriented resource for the analysis of systems-level datasets. Nat Commun. 2019;10(1):1523. https://doi.org/10.1038/s41467-019-09234-6

SUPPORTING INFORMATION

Additional supporting information can be found online in the Supporting Information section at the end of this article.